POLITECNICO DI TORINO
Repository ISTITUZIONALE

Vat photo-polymerization 3D printing of gradient scaffolds for osteochondral tissue regeneration

Original
Vat photo-polymerization 3D printing of gradient scaffolds for osteochondral tissue regeneration / Corrado, F., Di Maio, L., Palmero, P., Coppola, B., Abbas, Z., La Gatta, A., Schiraldi, C., Scarfato, P.. - In: ACTA BIOMATERIALIA. - ISSN 1742-7061. - 200:(2025), pp. 67-86. [10.1016/j.actbio.2025.05.042]

Availability:
This version is available at: 11583/3006787 since: 2026-01-21T14:39:49Z

Publisher:
Elsevier

Published
DOI:10.1016/j.actbio.2025.05.042

Terms of use:

This article is made available under terms and conditions as specified in the corresponding bibliographic description in the repository

Publisher copyright

(Article begins on next page)

07 November 2026

Acta Biomaterialia 200 (2025) 67–86

Contents lists available at ScienceDirect

Acta Biomaterialia

journal homepage: www.elsevier.com/locate/actbio

Review article

Vat photo-polymerization 3D printing of gradient scaffolds for osteochondral tissue regeneration

Federica Corrado [a], Luciano Di Maio [a], Paola Palmero [b], Bartolomeo Coppola [b], Zahid Abbas [b], Annalisa La Gatta [c], Chiara Schiraldi [c], Paola Scarfato [d,*]

[a] Department of Industrial Engineering, University of Salerno, Via Giovanni Paolo II n. 132, 84084 Fisciano, SA, Italy
[b] Department of Applied Science and Technology, Politecnico di Torino, INSTM R.U. Lince Laboratory, Corso Duca degli Abruzzi n. 24, 10129 Torino, Italy
[c] Department of Experimental Medicine, Section of Biotechnology, University of Campania "Luigi Vanvitelli", Via Santa Maria di Costantinopoli n.16, 80138 Napoli, Italy
[d] Department of Civil Engineering, University of Salerno, Via Giovanni Paolo II n. 132, 84084 Fisciano, SA, Italy

ARTICLE INFO

Keywords:
Vat photopolymerization
Stereolithography
Digital light processing
Osteochondral tissue regeneration
Gradient scaffolds

ABSTRACT

In recent decades, osteochondral (OC) tissue regeneration has been one of the major challenges in regenerative medicine. The absence of blood vessels, lymphatic vessels, and nerves in OC tissue prevents self-repair, while the structural complexity and differences between bone and cartilage layers make conventional surgical treatments largely ineffective. To address this issue, tissue engineering has emerged as a promising approach to replacing damaged OC tissue, with a particular focus on innovative strategies such as the design of continuous gradient scaffolds that mimic the complex architecture of native OC tissue. In this review vat photopolymerization (VPP) 3D printing technologies are presented as one of the most effective methods for fabricating gradient scaffolds for OC tissue repair. By leveraging photochemical reactions and light-assisted techniques, such as digital light processing (DLP), stereolithography (SLA) and two-photon polymerization (2-PP), highly precise porous structures made of biocompatible photo-crosslinkable resins have been successfully fabricated, with several relevant examples reported herein. DLP, SLA and 2-PP have proven fundamental in creating compositional, architectural, and mechanical gradients within scaffolds. Moreover, scaffold functionalization with bioactive molecules has demonstrated effectiveness in repairing damaged OC tissue in both *in vitro* and *in vivo* conditions. Moreover, the adoption of modeling tools such as the design of experiments (DoE) approach and AI-driven computational methods has proven to be valuable in optimizing the fabrication process and enhancing scaffold designs to more closely replicate the architecture and functionality of osteochondral tissues.

Statement of significance: Despite the transformative potential of vat photopolymerization (VPP) techniques, such as stereolithography (SLA) and digital light processing (DLP), for developing high-precision gradient 3D scaffolds for osteochondral (OC) tissue repair, achieving full biomimetic restoration remains a significant challenge. This review offers a comprehensive analysis of advancements in VPP, detailing how these techniques enable precise control over scaffold composition, architecture, and mechanical properties to closely replicate the complex structure of OC tissue. Furthermore, it underscores the critical need for standardized protocols and long-term evaluations in scaffold development. Addressing these gaps is essential to advancing the clinical translation of VPP-based scaffolds, paving the way for more effective treatments for OC tissue damage.

1. Introduction

Osteochondral (OC) tissue regeneration is one of the major challenges in regenerative medicine. In recent decades, research on OC tissue repair has increased significantly. A Scopus search using the keywords "osteochondral tissue" and "repair" in the "Article Title, Abstract, and Keywords" section identified >2500 studies on the latest advancements in the field (Fig. 1a). Refining the search with the terms "osteochondral" and "scaffolds" revealed over 1900 studies specifically focused on tissue engineering approaches aimed at fabricating and optimizing 3D structures for OC tissue regeneration (Fig. 1b). These studies explore various additive manufacturing techniques and different

* Corresponding author.
E-mail address: pscarfato@unisa.it (P. Scarfato).

https://doi.org/10.1016/j.actbio.2025.05.042
Received 9 January 2025; Received in revised form 15 April 2025; Accepted 16 May 2025
Available online 23 May 2025
1742-7061/© 2025 The Authors. Published by Elsevier Inc. on behalf of Acta Materialia Inc. This is an open access article under the CC BY license (http://creativecommons.org/licenses/by/4.0/).

biomaterials to develop scaffolds that effectively replicate the physicochemical properties of native OC tissue. Research has increasingly shifted from simple structures, designed to mimic only specific parts of the multiphasic OC tissue, to more complex architectures, with 3D printing emerging as one of the most promising approaches. However, the attention of the scientific community was predominantly focused on OC gradient scaffolds produced using techniques based on extrusion and sintering processes, such as fused deposition modeling (FDM) and selective laser sintering (SLS). While these methods yield scaffolds with good performance, they often lack well-defined structures with high resolution. On the other hand, limited attention has been dedicated to light-assisted techniques, which utilize light sources to build scaffolds made of photo-crosslinkable materials. In this context, advanced techniques such as stereolithography (SLA) and digital light processing (DLP) offer significant advantages, enabling precise control over the resolution, physicochemical characteristics, and mechanical properties of the scaffolds [1–5].

This review aims to emphasize the importance of light-assisted techniques in the fabrication of OC gradient scaffolds, highlighting their ability to create gradients in architecture, geometry (pore shape, pore size, and pore openings), composition (blends of natural and synthetic polymers combined with inorganic materials in different ratios), and mechanical properties (stiffness, compressive strength, etc.). Additionally, this review underscores the advantages of these techniques, including their capacity to produce complex and highly detailed scaffold structures at high printing speeds, as well as the ability to manufacture large batches of scaffolds with varying geometries and surface finishes. Another key objective is to collect information that serves as an overview for selecting suitable materials, such as matrices and photoinitiators, and optimizing process parameters for the fabrication of gradient scaffolds using SLA, DLP and 2-PP techniques. To conduct this review, Scopus and PubMed were used as the primary databases for sourcing peer-reviewed studies, while Google Scholar was used to expand and enrich the research. The main keywords employed in the search included: gradient, osteochondral, scaffolds, stereolithography, digital light processing, and vat photopolymerization processes.

2. Scaffolds for osteochondral tissue engineering

2.1. Osteochondral tissue anatomy

Osteochondral (OC) tissue is a specialized structure located at the interface between bone and articular cartilage, playing a crucial role in providing structural support, bearing weight, reducing friction, and cushioning movements. These functions are made possible by its complex, multilayered architecture, which can be broadly divided into three main regions: non-calcified cartilage (hyaline cartilage), calcified cartilage, and the subchondral zone [6]. The non-calcified cartilage can be further subdivided into three layers: the superficial zone, the middle zone, and the deep zone, each exhibiting gradual variations in cell shape, size, and orientation (chondrocytes), extracellular matrix (ECM) composition (collagen, water, and mineral content), and mechanical properties such as stiffness and compressive strength (Fig. 2a) [7–10].

Since OC tissue is directly involved in joint movement, it is particularly vulnerable to damage. Injuries to OC tissue, known as osteochondral defects (OCDs), arise from traumatic events, repetitive microtrauma, or conditions like osteochondritis, ultimately compromising joint function [11,12]. Addressing these defects represents a major challenge in orthopedic medicine, due to the complex layered structure of OC tissue, combined with its limited vascularization and innervation, that hinders self-repair [13]. Current treatment strategies for OC damages are often palliative cares which impart only symptomatic relief without preventing further degeneration [5,14,15]. More advanced approaches involve surgical reparative and restorative procedures, such as autologous chondrocyte implantation (ACI), which can effectively reduce pain in the short term and promote regeneration of the OC tissue, [16,17]. However, these approaches are limited by risks of infection and immunogenic responses [14,18,19]. In recent years, tissue engineering has emerged as a promising alternative for OC tissue repair by integrating principles from biology, materials science, and engineering to develop innovative regenerative strategies [20–22]. Indeed, by designing biodegradable and biomimetic scaffolds and incorporating growth factors and stem cells into the structure, it is possible to provide biomimetic mechanical support, and promote cellular diffusion, growth, and differentiation, ultimately accelerating OC tissue regeneration [23, 24].

2.2. Manufacturing and architectures of scaffolds for osteochondral regeneration

2.2.1. Manufacturing techniques

Tissue engineering is currently recognized as the most effective alternative to conventional treatments for OC tissue regeneration [25]. Using a multidisciplinary approach, it aims to develop cell-laden scaffolds (constructs) designed for *in vivo* implantation, where they temporarily replace the damaged/lost tissue while promoting its regeneration [26].

As a key requirement, the scaffold should serve as an artificial ECM by properly interacting with the cell component, supporting cell adhesion, proliferation, and, in the case of stem cells, differentiation. At the

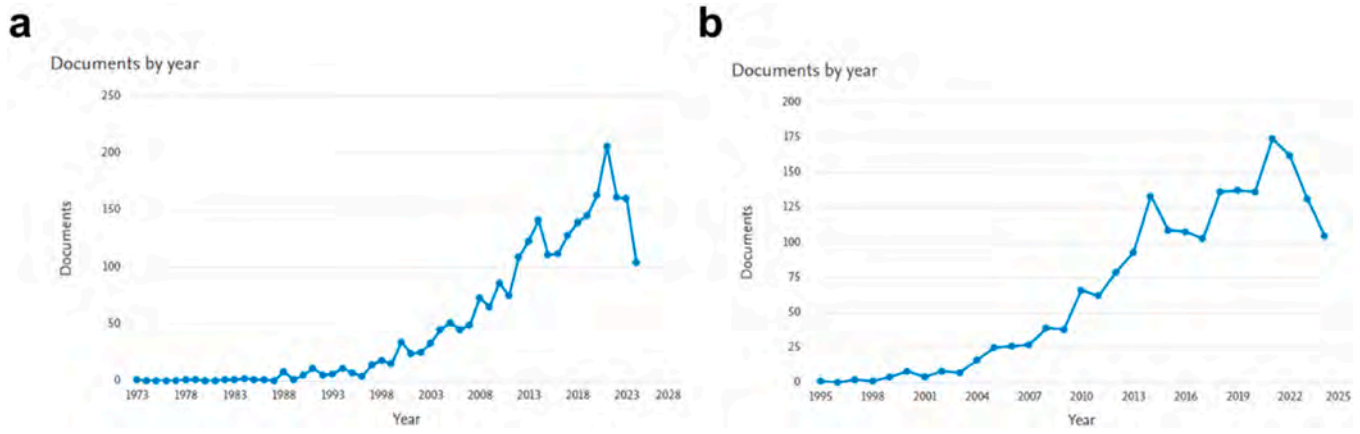

Fig. 1. Graphs obtained by Scopus search (accessed in July 2024) showing the number of studies carried out over the last years. a) The first graph reports the number of works from 1973 to 2024 by using the keywords "osteochondral tissue" and "repair" showing how the topic is still of interest nowadays, with an exponential focus in the last 30 years. b) The second graph reports the number of papers written from 1995 to 2024 by using the terms "osteochondral" and "scaffolds" depicting the growing interest in tissue engineering approaches for OC tissue repair.

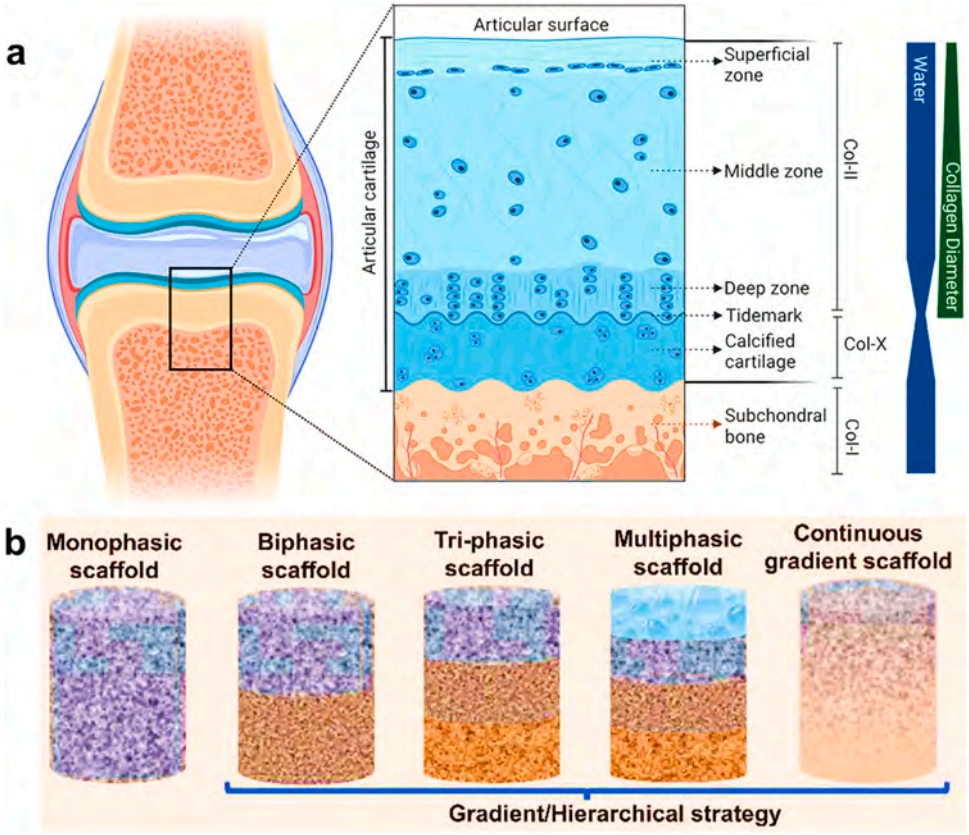

Fig. 2. Schematics of osteochondral tissue and tissue engineering approaches. a) Schematic representation of the gradient osteochondral tissue: articular noncalcified cartilage (divided into superficial zone, middle zone, and deep zone), calcified cartilage, and subchondral bone and their composition. The wide and gradual extracellular matrix (ECM) composition change is depicted. Reproduced and adapted with permission from Ref. [7]. Copyright 2019, MDPI; b) Schematic representation of tissue-engineered scaffold for osteochondral tissue repair: several approaches based on the number of layers and properties of the scaffold are shown, moving from monophasic to continuous gradient structures. Reproduced and adapted with permission from Ref. [5]. Copyright 2023, Elsevier.

same time, they must provide adequate structural and mechanical support. Further, a scaffold degradation profile matching the rate of new tissue formation is highly desirable. To effectively guide tissue development, scaffolds must replicate the natural ECM in terms of chemical composition, mechanical properties, and structural features, including porosity, pore interconnectivity, and a multiscale three-dimensional architecture spanning the macro-, micro- and nano-levels. This ensures that cells receive the necessary biochemical and biophysical cues for proper tissue formation. Regardless of the specific technology employed for OC scaffold production, the past decades have seen significant advancements in scaffold chemical composition and mechanical properties, leading to greater biomimicry through the incorporation of natural ECM components. Also, significant progress has been made in developing biomimetic 3D scaffold architectures that more closely resemble the ECM of bone and cartilage, particularly thanks to additive manufacturing (AM) technologies [26–28].

Various AM techniques have been developed to fabricate these scaffolds by depositing materials at specific spatial coordinates along the gradient axis. These include sequential layering of partially gelated hydrogel solutions, electrospinning, freeze-drying, microfluidic-based techniques, magnetic field-assisted methods, and 3D printing [5,29–41]. Among these, 3D printing is the most widely used and promising approach. It is supported by computer-aided design (CAD) which allows designing scaffolds with customized and complex architecture. The fabrication process typically involves layer-by-layer deposition techniques, providing precise control over the chemical composition, geometry, and mechanical properties of each layer. In addition, 3D printing offers the possibility of incorporating biological substances, such as growth factors or inorganic components naturally present in OC tissue, which enhance cell attachment, spreading, and the chondrogenic and osteogenic differentiation of stem cells [5]. Depending on the material used and the working principle of the technique, the most common methods include fused deposition modeling (FDM) or fused filament fabrication (FFF), which utilize extrusion technology, selective laser sintering (SLS) based on powder fusion, and light-assisted techniques, such as vat photopolymerization (VPP) [42]. VPP relies on photochemical reactions and includes methods like SLA, DLP, and two-photon polymerization (2-PP) [4,43]. A comparison of these 3D manufacturing techniques is reported in Table 1 [2,44].

The FDM or FFF technique, illustrated in Fig. 3a, operates by extruding a molten filament of thermoplastic material through the heated nozzle of a printer head under pressure. The extruded filament is deposited layer by layer onto a build platform. After the first layer is laid down, the printer head moves along the Z-axis, while the nozzle continues depositing material along the X and Y axes to form subsequent layers. As the material cools and solidifies, the process repeats until the entire scaffold is completed [45]. The SLS method, depicted in Fig. 3b, utilizes a high-energy source, such as a laser, to sinter powdered materials. A mirror directs the laser beam onto the powder bed, heating and fusing the particles through a sintering process. After each layer is formed, a new layer of powder is added to the chamber, and the process repeats until the scaffold is fully constructed [46].

Another promising technology for OC scaffold fabrication is 3D bioprinting [47]. This method incorporates principles from previously mentioned techniques, including extrusion-based, inkjet-based, and laser-assisted approaches (Fig. 3c). However, unlike traditional AM methods, bioprinting deposits bioinks, even highly viscous, composed not only of biomaterials but also of living cells and biochemical factors,

Table 1
Comparison of 3D manufacturing techniques (information were derived from Refs. [2,44]).

Technique	Advantages	Limitations	Applications	Biomaterial Compatibility	Minimum feature size	Printing Speed
Fused Deposition Modeling (FDM)	Low cost, easy to use, customizable porosity	Limited resolution, anisotropic mechanical properties	Bone tissue engineering, cartilage scaffolds	Biocompatible thermoplastics (PLA, PCL, ABS, PGA)	60–600 μm	Moderate
Fused Filament Fabrication (FFF)	Similar to FDM, cost-effective, accessible	Poor surface quality, lower resolution than SLA or SLS	Biodegradable polymer scaffolds, custom implants	Biocompatible thermoplastics (PLA, PCL, PGA)	50–500 μm	Moderate
Selective Laser Sintering (SLS)	No need for support structures, strong and porous structures	High energy consumption, rough surface finish	Bone and cartilage scaffolds, tissue engineering	Polymers (PA, PCL), metals (Ti, Co-Cr)	100–1000 μm	Moderate
Stereolithography (SLA)	High resolution, smooth surface, precise microstructures	Expensive resins, requires post-curing, brittle materials	Soft tissue scaffolds, microvascular networks	Photopolymer resins, PEGDA-based biomaterials	10–100 μm	High
Digital Light Processing (DLP)	Faster than SLA, high accuracy, smooth surfaces	Limited material choices, requires post-processing	Bioprinting, vascularized scaffolds	Biocompatible resins, PEG-based hydrogels	10–100 μm	High
2-Photon Polymerization (2-PP)	Extremely high resolution, complex 3D microstructures	Expensive, slow, small build volume	Nerve regeneration, cell-laden hydrogel scaffolds	Photosensitive biomaterials, hydrogels, PEGDA	0,1–0,7 μm	Low

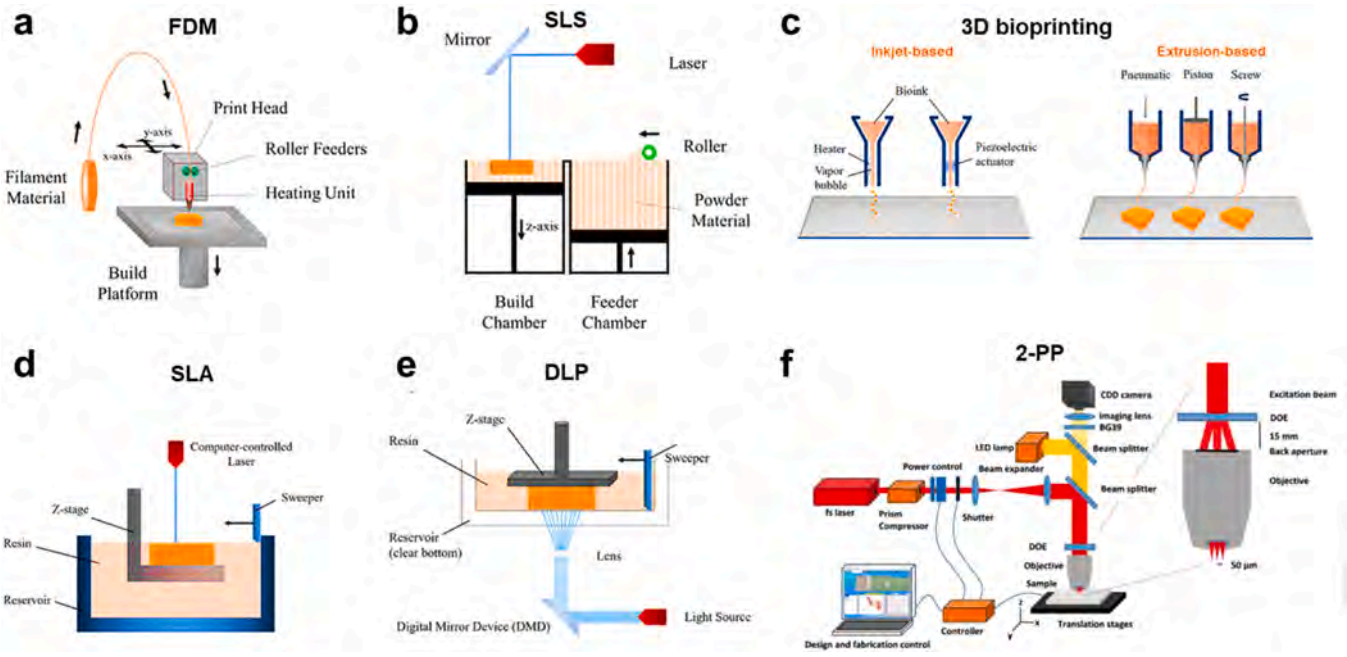

Fig. 3. Schematic representation of the most common additive manufacturing (AM) 3D printing techniques. a) Fused deposition modelling (FDM). FDM operates by extruding material through a heated nozzle under pressure to create 3D printed scaffolds. Polymeric materials are melted producing fibrous filaments deposited layer-by-layer on a stage, with the nozzle moving along the vertical gradient axis; b) Selective laser sintering (SLS). A laser heats and blends powders contained in a mold. After the first layer deposition, a new one is added by a piston and undergoes sintering to form the subsequent layer. This process repeats until the vertical gradient scaffold is achieved. c) 3D bioprinting techniques. Inkjet-based 3D printing: an ink or bioink is placed into a cartridge and can be dispensed using heat-generated bubbles or a piezoelectric actuator. Extrusion-based 3D printing: the bioink is extruded using pneumatic or mechanic (piston/screw) systems. d) Stereolithography (SLA). A transparent reservoir contains liquid photopolymer resin. Each layer is traced onto the surface of the resin by a computer-controlled laser that directs the beam in the X and Y direction where solidification is needed. When the laser hits the liquid resin, it starts to cure and then solidifies, forming the desired shape of the first layer. After one layer is solidified, a stage holding the hardened material moves downwards vertically by a small distance and the tank is re-filled with a fresh liquid resin. This process repeats until the entire object is achieved. e) Digital light processing (DLP). A large array of microscopic mirrors arranged in a grid rotates to be in an "on" or "off" position. When the micromirrors are in the "on" position and are hit by light, they reflect it to produce an image. Micromirrors in the "off" positions are oriented to avoid the incident light. Consequently, light reflected by the mirrors is directed toward the resin, which is then illuminated and polymerized, resulting in a solidified material with the same shape as the projected image. Reproduced and adapted with permission from Ref. [42]: Copyright 2021, MDPI. f) 2-Photon Polymerization (2-PP). The absorption of photons in the near-infrared (NIR) spectrum triggers the photopolymerization and, thus, the solidification of the liquid material only where the light intensity is the highest also known as the focal point. The focal point is moved by galvo scanners in the focal plane at speeds of hundreds of millimeters per second and the laser beam is focused into the photosensitive resin using a high numerical aperture objective lens. Reproduced and adapted with permission from Ref. [43]: Copyright 2020, "Scientific" Reports.

enabling the fabrication of large, mechanically stable structures with high resolution and precision. Nevertheless, bioprinting poses challenges such as shear stress on cells, which can reduce cell viability, as well as high costs and technical complexity. Despite these limitations, bioprinting continues to evolve rapidly, with ongoing research focused on improving bioink formulations, developing hybrid printing techniques, and integrating artificial intelligence to optimize printing parameters. Although still in its early stages, bioprinting holds great

potential for tissue regeneration, paving the way for future breakthroughs in biomedical engineering.

VPP techniques (Fig. 3d-f) are 3D printing technologies that use ultraviolet (UV), infrared (IR), or visible light. These systems leverage light as an energy source and apply photochemistry principles and advanced fabrication techniques to design OC scaffolds. The process involves photo-crosslinkable liquid materials (resins) contained in a tank, which are selectively crosslinked by a light source at a precise wavelength to form each layer of the scaffold. This approach, through precise control of the processing parameters (*i.e.*, light source wavelength and intensity, exposure time), enables the fabrication of nanoscale features with enhanced resolution and allows for the accurate customization and fine-tuning of the scaffold geometry, zonal-specific composition, 3D architecture, and mechanical properties [43,44].

A detailed discussion of the working mechanisms, advantages, and limitations of these technologies is provided in Section 2, *Vat Photopolymerization (VPP) Techniques*.

2.2.2. Types of scaffolds' architectures

To effectively build scaffolds that replicate the natural intricate structure of OC tissue, it is essential to mimic the mechanical and physicochemical characteristics of non-calcified cartilage, calcified cartilage, subchondral bone, and their interfaces within a single construct with the highest precision. Consequently, in recent years, increasing attention has been devoted to the evolution of OC scaffold design, moving from simple monophasic structures to more sophisticated architectures, including bi-layered, multi-layered, and continuous gradient scaffolds (Fig. 2b) [1,3–5].

In the following, a concise overview of the main architectures and temporal progression of the different types of scaffolds will be provided, highlighting the advancements made in their development to enhance biomimicry and integration with native osteochondral tissue.

2.2.2.1. Mono-layered scaffolds. Mono-layered scaffolds were the first type of constructs developed for OC tissue restoration. These structures are designed to interact with a single phase of the tissue (*e.g.*, either bone or cartilage) at a time, promoting cell attachment and proliferation within the defected area. They are typically composed of a single material or a homogeneous mixture of multiple materials, with uniform spatial distribution and isotropic mechanical and physicochemical properties [5,7,50].

Common materials used for scaffold fabrication include natural polymers such as carbohydrates (agarose, alginate, chitosan/chitin, and hyaluronate) and proteins (collagen, fibrin, and gelatin), as well as synthetic polymers like polyglycolic acid (PGA), polylactic acid (PLA), poly(lactic-co-glycolic acid) (PLGA), polyethylene glycol (PEG), and

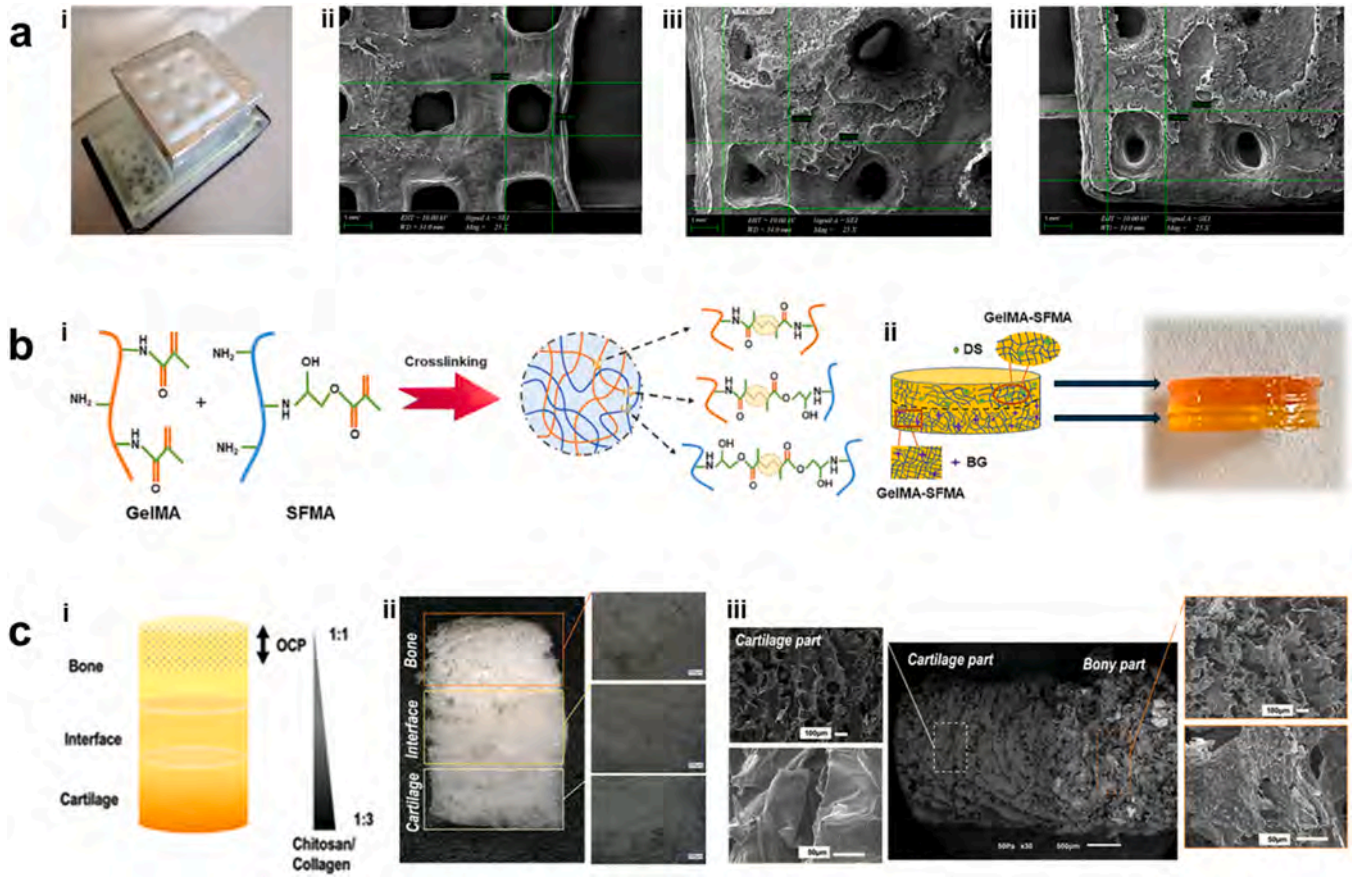

Fig. 4. Representation of mono-layered, bi-layered and three-layered scaffolds obtained by VPP techniques. a-i) picture of a DLP printer component with a mono-layered printed scaffold. a-ii) SEM image from the surface of GelMA hydrogels scaffold. a-iii) SEM image from the surface of GelMA composite hydrogels (GelMA-HA-PR-Sr10 %) scaffold. a-iiii) SEM image from the surface of GelMA composite hydrogels (GelMA-HA-HT-Sr10 %) scaffold. Reproduced and adapted with permission from Ref [53]. Copyright 2024, MDPI. b-i) Schematic representation of crosslinking reaction between gelMA and SFMA to obtain GelMA-SFMA hydrogel. b-ii) Schematic representation and related picture of bi-layered GelMA-SFMA hydrogel scaffold in which the upper layer, enriched with diclofenac sodium (DS), mimics the cartilage layer, while the bottom layer, loaded with bioactive glass (BG), mimics the subchondral bone part. Reproduced and adapted with permission from Ref [69]. Copyright 2023, Springer Link. c-i) Schematic representation of the three-layered chitosan-collagen-octacalcium phosphate scaffold. Different zones and material composition are identified. c-ii) Digital light microscopy images showing the different zones in the three-layered scaffold. The layers of the scaffold corresponding to the bone, interface, and cartilage regions are indicated by colored boxes added to the images. c-iii) SEM images illustrating the microstructure and morphological features of the obtained scaffolds. Reproduced and adapted with permission from Ref [79]. Copyright 2021, Wiley.

polycaprolactone (PCL) [51]. To enhance mechanical properties, natural polymers are often blended with synthetic ones or combined with inorganic fillers such as hydroxyapatite (HA) and tricalcium phosphate (TCP) [47].

One of the earliest examples of mono-layered scaffolds was reported by Cao et al. in 2003. They investigated the use of a three-dimensional isotropic porous PCL scaffold fabricated via FDM, demonstrating its potential for osteochondral repair applications [52]. Even today, mono-layered structures continue to be developed. A recent example is the work of Codrea et al. in 2024, who fabricated various DLP-printed mono-layered scaffolds composed of GelMA (Fig. 4a-i and ii) and GelMA-strontium doped with hydroxyapatite (Fig. 4a-iii and iiii) [53]. By varying the matrix composition, they achieved different pore structures, effectively mimicking bone tissue and promoting its regeneration. Additionally, mono-layered scaffolds primarily composed of bioceramics have shown promising results in bone regeneration. In particular, VPP techniques have demonstrated significant potential for fabricating bioceramic scaffolds with precise control over geometry and porosity, enabling the creation of intricate, biomimetic structures. These techniques facilitate the integration of bioactive ceramics such as HA, whitlockite, and bredigite-doped composites in the scaffolds, improving mechanical strength, degradation behavior, and biological responses [54–56].

Although monophasic scaffolds remain in development due to their relatively simple fabrication process, they are inherently limited in replicating the complex physical structure and functional properties of OC tissue required for its effective repair. Consequently, they fail to fully recreate the biological environment necessary for complete OC tissue regeneration. To overcome these limitations, researchers have explored scaffolds that incorporate two distinct joint phases, offering a more advanced and biomimetic approach.

2.2.2.2. Bi-layered scaffolds. Bi-layered scaffolds are the first example of stratified constructs able to mimic the biological environment of the different layers in native OC tissue by varying chemical composition, structural arrangement, and mechanical properties. They were specifically designed to independently replicate the native ECM of both bone and cartilage within a single scaffold. These scaffolds can be composed of two distinct materials forming separate layers, which are either integrated through a mutual material common to both layers or joined using an artificial interface, such as fibrin glue. Alternatively, a single material can be used exhibiting two different structural arrangements [57].

Numerous studies have demonstrated that, compared to monophasic scaffolds, bi-layered constructs provide a more suitable environment for guiding interactions with the matrix, providing the necessary chemical, mechanical, and biological stimuli to promote both chondrogenic and osteogenic proliferation in OC and bone tissues [58]. Common materials used to mimic the bone phase are synthetic polymers (PCL, PLA, PLGA), ceramics (HA and TCP), bioactive glasses and demineralized bone particles, while cartilage is generally simulated by soft natural polymers such as collagen, gelatin, chitosan, alginate, hyaluronic acid, silk-fibroin and chondroitin sulfate [59–67]. The combination of natural and synthetic polymers allows for fine-tuning the mechanical properties of the scaffolds. Furthermore, their biological performances can be enhanced through matrix functionalization or by incorporating biomolecules, such as growth factors.

One of the first examples of a bi-layered scaffold combining two different materials was reported by Guo et al. in 2009. They developed a composite scaffold of oligo(poly(ethylene glycol) fumarate) (OPF) hydrogel with gelatin microparticle, and TGF-β1 as a growth factor to emulate the structure and function of bone and cartilage tissues [68].

A more recent example of a bi-layered scaffold was developed by Zhao and colleagues [62]. They created a bilayer construct composed of copolymerized GelMA and methacrylated silk fibroin (SFMA), which was then 3D printed using the DLP technique via a crosslinking reaction (Fig. 4b-i). To enhance the scaffold's reparative efficacy for cartilage defects, diclofenac sodium (DS) was incorporated into the cartilage-mimicking layer as a model anti-inflammatory agent, while bioactive glass (BG) was loaded into the bottom subchondral bone layer to promote new bone regeneration (Fig. 4b-ii) [69].

However, even though bi-layered scaffolds more effectively mimic the microenvironment of both tissues better than mono-layered ones, they don't include calcified cartilage, and do not fully replicate every gradient present in OC tissue. To address this limitation, more complex biomimetic scaffolds with three or multiple layers have been developed.

2.2.2.3. Multi-layered scaffolds. Unlike the previously mentioned architectures, triphasic and multiphasic scaffolds incorporate the calcified cartilage layer of OC tissue. This crucial layer serves as a transition between soft cartilage and stiff subchondral bone, playing a key role in converting shear stresses into compressive and tensile stresses during joint movement [3,5,70]. To mimic the calcified cartilage structure, various combinations of materials, including HA, bioglasses, alginate, and collagen, are finely blended to achieve properties that closely resemble those of native tissue [71–73]. One of the earliest examples of a three-layered OC scaffold was developed by Tampieri et al. in 2008. Their design consisted of distinct layers of collagen, hydroxyapatite, and chondroitin sulfate, specifically structured to replicate native osteochondral tissue, including the calcified cartilage layer. This scaffold showed promising results in supporting mesenchymal stem cell growth and differentiation *in vitro* [74].

While triphasic scaffolds successfully mimic articular cartilage, calcified cartilage, and subchondral bone, they do not fully replicate the gradual transition of properties between these layers. To address this limitation, multiphasic scaffolds have been developed, incorporating discrete layers joined into a single structure using time-consuming techniques such as suturing, gluing, and press-fitting [75–78].

More recently, Amann *et al.* explored the fabrication of complex multilayer scaffolds composed of chitosan, collagen, and octacalcium phosphate (OCP). In these constructs, the OCP content is higher in the bone-mimicking region, while collagen concentration increases progressively toward the cartilage layer, with OCP content decreasing accordingly (Fig. 4c-i, 4c-ii and 4c-iii) [79]. However, despite eliminating clearly defined interfaces between individual layers, multilayered scaffolds still face challenges related to layer delamination and tissue separation [80].

To mitigate these structural weaknesses, a significant advancement in OC tissue engineering has been the shift towards monolithic structures, which eliminates the need for additional junctions. In this context, the development of continuous gradient scaffolds has gained increasing attention [4]. Currently, gradient OC scaffolds represent the most promising approach in clinical applications for OC tissue restoration [81,82].

2.2.2.4. Gradient scaffolds. Gradient scaffolds are designed with gradually changing characteristics, such as chemical composition, geometry, density, porosity, and mechanical properties, within a single continuous structure, eliminating discrete layers and more closely mimicking the natural composition and features of OC tissue [4]. Compared to traditional scaffolds, the continuous property transitions in gradient scaffolds enhance nutrient diffusion, promote cell adhesion, viability, and differentiation, and improve mechanical stability [4,83]. For example, Karimi et al. developed OC gradient scaffolds using FDM with three different compositions of hydroxyapatite (HA) and poly(ε-caprolactone) (PCL). Their study demonstrated improved morphological similarity to cortical bone and enhanced biological activity [84]. Di Luca et al. monitored the proliferation, differentiation, and ECM deposition of human mesenchymal stem cells (hMSCs) seeded within a scaffold fabricated by an FDM method featuring a porosity gradient. Their

findings revealed enhanced chondrogenic gene expression and increased glycosaminoglycan (GAG) deposition compared to non-gradient scaffolds. Based on their results, they concluded that structural gradients represent a promising strategy for designing scaffolds that support and enhance the chondrogenic differentiation of adult stem cells [4].

In recent years, SLS technology has also made decisive steps in the fabrication of gradient OC scaffolds [29,85–89]. Du et al., for example, used SLS to create a gradient scaffold composed of PCL and HA microspheres, which was then implanted into a rabbit model to treat osteochondral defects. Their findings revealed that the scaffold effectively supported subchondral bone regeneration, integrated well with native tissues, and encouraged the formation of articular cartilage [29].

Lately, Gu et al. fabricated by SLS three types of PCL microsphere-based scaffolds with different channel patterns (Non-channel, Consecutive-channel, and Inconsecutive-channel) to optimize structural integrity and mechanical properties. Their research demonstrates that the inconsecutive-channel hierarchical structure, having gradient interconnected porosity, effectively supports osteochondral reconstruction enhancing nutrient diffusion and cell infiltration, providing adaptable compressive strength, and facilitating bone ingrowth and vascularization [89].

Although SLS and FDM methods offer cost-effective solutions for fast manufacturing of OC gradient scaffolds, they produce constructs with relatively low resolution [90]. Moreover, they tend to generate substantial material waste [91]. In fact, SLS works by selectively sintering powdered materials layer by layer, requiring an excess amount of powder to surround the printed object. While some of this powder can be reused, material degradation over multiple cycles limits its recyclability, leading to significant waste accumulation. Similarly, FDM operates by extruding thermoplastic filaments through a heated nozzle, often requiring support structures that must be removed post-printing, contributing to material waste.

In contrast, VPP techniques, which use liquid resins that can be selectively cured with high precision, allow for micron- and sub-micron-level precision, achieving the highest printing resolution and an exceptional control over scaffold characteristics, such as porosity, permeability, pore size, shape, and interconnectivity [2,86]. The capability to accurately replicate the micro/nanotopographical cues of the extracellular matrix provides the potential to influence stem cell adhesion, morphology, and differentiation through mechanotransduction pathways and regulatory mechanisms critical for tissue regeneration [93]. Moreover, the uncured resin in the vat remains reusable for subsequent prints, minimizing material consumption and waste. However, they also have some drawbacks, such as longer print times and the need for continuous resin replenishment in the tank. Nevertheless, ongoing advancements in ink formulations and technological refinements are actively addressing these challenges, further enhancing their potential for OC tissue engineering.

In the following section, the vat photo-polymerization techniques for 3D printing of gradient scaffolds are reviewed in detail.

3. Vat photo-polymerization (VPP) techniques for 3D printing of continuous gradient scaffolds

Vat photopolymerization techniques for fabricating 3D constructs for osteochondral tissue regeneration include several methods, like SLA, DLP, and 2-PP. The following sections provide a detailed review of literature on them, tracing the development of VPP-based continuous gradient scaffolds from their earliest prototypes to the latest advancements. A summary of all the reviewed studies is provided in Table 2. To offer a more intuitive overview, a spider chart (Fig. 5) has been also included, visually representing the relative strengths and limitations of each technique across key parameters relevant to osteochondral scaffold fabrication. In addition to mathematical modeling, which serves as the initial approach for designing OC gradient scaffolds, the discussion also explores the integration of predictive software in scaffold development.

3.1. Stereolithography (SLA)

SLA was the first VPP technique ever developed, introduced by Charles Hull in the mid-1980s [94]. The SLA process begins with the design of a 3D CAD model, which is then sliced into thin layers using specialized software. The SLA equipment is shown in Fig. 3dA transparent tank holds liquid photopolymer resin. A laser, controlled by Galvo scanners, traces each layer onto the surface of the liquid photopolymer. These scanners direct the laser along the X and Y axes, precisely targeting the locations within the resin tank where solidification is required. When the laser strikes the liquid resin, polymerization occurs, causing the liquid resin to cure and solidify, forming the first layer of the scaffold. Once a layer is solidified, the build platform lowers incrementally, allowing a fresh layer of liquid resin to coat the previous one. This process repeats layer by layer until the entire object is formed. Once the printing process is complete, the object is removed from the printer and cleaned to remove resin excess. Sometimes, a post-curing process is performed, usually involving UV light, to strengthen the material [92].

Porosity is a key feature to be optimized to better replicate the OC tissue's structure. It facilitates nutrients and cellular diffusion, and waste removal. In this regard, SLA-made scaffold can be designed and fabricated with precise control over pore shape and size. For this purpose, Melchels et al. proposed one of the first mathematical model of an OC gradient scaffold made by SLA technique, in which porosity ranged from 70 % at the mid-section to 30 % at the bottom end of the structure [95]. On the basis of the model, the researchers fabricated SLA 3D-printed scaffolds with gyroid-shaped pores. Unlike the tortuous pore architecture typically produced by conventional additive manufacturing methods, which can hinder cell medium accessibility, the well-defined gyroid shape and interconnected pores facilitated uniform nutrient and oxygen diffusion, leading to homogeneous cell distribution and viability after seeding [96]. Later, they developed two different biodegradable scaffold types made of PDLLA-MA with the same gyroid pore architecture but differing in of pore size distribution (Fig. 6a and b). One design exhibited isotropic pore size, and the other had a gradient in pore size (ranging from 250 μm to 500 μm) and porosity (ranging from 35 % to 85 %), effectively mimicking the natural gradient porosity of OC tissue [97]. Human articular chondrocytes were cultured within both scaffolds. Isotropic scaffolds displayed a uniform distribution of cell densities after seeding, whereas scaffolds engineered with a gradient in pore size and porosity exhibited directional variations in adherent cell densities. Indeed, authors found the highest densities of cells in the scaffolds' regions where the pores were larger. In both studies, variations in porosity and pore size also resulted in corresponding gradients in stiffness and permeability. Specifically, as porosity increased, stiffness decreased due to reduced solid material providing structural support, while permeability increased, allowing for enhanced fluid transport velocities across the scaffold. This created functional gradients within the scaffold [95,97].

Aiming to improve OC scaffold performances, Bian et al. performed histological analysis of OC tissue, focusing on both its morphological characteristics and the binding forces at the interface between cartilage and bone phases (Fig. 6c-i) [98]. Based on the obtained findings, they designed a multiple-layered scaffold made of an acrylamide matrix loaded with β-tricalcium phosphate (β-TCP) and type I collagen to mimic the bone phase, cartilage phase, and their transitional structure, as shown in Fig. 6c-ii. In particular, the researchers combined two different AM techniques, a custom-made ceramic stereolithography (CSL) and gel casting, successfully recreating a scaffold that mimicked the porosity and mechanical properties of native OC tissue [98]. The resulting structure featured a highly porous and interconnected channel structure, with final pore sizes of 700 μm - 900 μm and diameters of the interconnected pores between 200 μm and 500 μm, while the compressive strength was 12.4 MPa ± 0.5 MPa. They also measured a shearing resistance of 11.8 N ± 1.6 N between the layers, closely matching the binding forces of native OC tissues [98]. However, this study had some

Table 2
Summary of the articles reported in literature about OC gradient scaffolds made by VPP techniques, sorted by year of publication. In the table, the main results of the discussed articles are reported, enriched with process parameters and materials used to obtain the gradient OC scaffold. Moreover, also the mimicked tissue and type of gradient are presented with a brief mention about cells or animal model used for the *in vitro* and *in vivo* tests.

Reference (Year)	Tissue	Technique and process parameters	Materials	Type of gradient	Test *in vitro or in vivo*	Main results
Melchels et al. (2010) [95]	Bone OC	SLA PI = Lucirin TPO-L λ = blue light $P = 16$ mW/cm^2 $t = 30$ s	PDLLA and P(DLLA-co-CL) Methacrylated Photoabsorber: Orasol Orange G dye Inhibitor: α-tocopherol	Porosity	Not evaluated	First mathematical model of OC gradient scaffold made by SLA technique. Scaffold with gyroid pore architecture with a gradient in pore size and porosity (ranged from 70 % at the mid-section to 30 % at the bottom end of the structure).
Melchels et al. (2010) [96]	Bone OC	SLA PI = Lucirin TPO-L λ = blue light $P = 16$ mW/cm^2 $t = 30$ s	PDLLA Methacrylated Photoabsorber: Orasol Orange G dye Inhibitor: α-tocopherol	Porosity	Human articular chondrocytes	Scaffold with gyroid pore architecture with a gradient in pore size and porosity: gradient in pore size ranged from 250 μm to 500 μm while porosity ranged from 35 % to 85 %. Articular chondrocytes exhibited directional variations in adherent cell densities.
Bian et al. (2012) [98]	Bone Cartilage Transitional structure OC	Ceramic stereolithography (CSL) = β-TCP + acrylamide PI = photocure-1173 λ = 355 nm $P = 220$ mW Scan speed = 2000 mm/s Gel casting and freeze drying = type I collagen	Bone = β-TCP in acrylamide Cartilage = Type I collagen	Porosity	Bone marrow stromal cells (MSCs)	Histological analysis of OC tissue on morphological characteristics and binding forces at the interface between cartilage and bone phases. Two different AM techniques (CSL and gel casting) were used to recreate the different layers. Diameters of pore ranged from 200 μm to 500 μm. Compressive strength was found 12.4 ± 0.5 MPa. Shearing resistance was of 11.8 ± 1.6 N between the layers showing a binding force very similar to the one found in OC tissue.
Castro et al. (2015) [99]	OC	Table-top SLA PI = BAPO λ = 355 nm $P = 40$ −110 mW/cm^2 Printing speed = 2000 mm/min	Bone = nHA + PLGA nanospheres + TGF-β_1 Cartilage = PEGDA	Composition Bioactive growth factor release	hMSCs	Gradient of nHA concentration from 10 % to 20 % to mimic the architecture and the mechanical properties of the subchondral bone layer. Improved and driven adhesion, proliferation, and differentiation of hMSCs due to the presence of TGF-β_1 growth factor.
Wu et al. (2018) [100]	OC	SLA PI = DAROCUR 1173, DAROCUR-TPO λ = 400 nm $P = 2.64$ - 14.98 mW/cm^2 $t = 3.5$ s	Bone = β-TCP in HDDA and PEG Cartilage = PEGDA	Composition at the interface	Not evaluated	Use of multi-material stereolithography (MMSL) technique with different light power densities to harden the materials with different curing characteristics. A strong interface between the materials was found strong enough to resist a separation force.
Zhou et al. (2019) [101]	OC	SLA PI = I2959 λ = 355 nm Printing speed = 10 mm/s	Subchondral tissue = gelMA + PEGDA + nHA Cartilage = gelMA + PEGDA + PLGA nanoparticles + TGF-β_1	Composition	Human bone marrow derived mesenchymal stem cells (hMSCs)	Gradient scaffold made of different ratios of gelMA and PEGDA. hMSCs were cultured into the scaffold showing induced osteochondrogenic proliferation and differentiation.
Chen et al. (2019) [105]	Cartilage	Desktop-SLA (DLP) PI = LAP λ = 405 nm $P = 11$ mW/cm^2 $t = 30$ s	MSC derived esosome + decellularized cartilage ECM + gelMA	Radially oriented channels Elastic modulus	Rabbits (*in vivo*)	Scaffold with radially oriented channel in which the pore size varied depending on the concentration of ECM used in the hydrogel mix from 91.6 ± 7.0 μm to 106.8 ± 6.9 μm while the Young's Modulus changed with increasing ECM concentration from 16.09 ± 0.56 kPa to 37.72 ± 2.82 kPa throughout the structure. Scaffold promoted cartilage regeneration, by restoring cartilage mitochondrial dysfunction and enhancing chondrocyte migration.
Xue et al. (2019) [109]	Promising for muscle and cartilage	DLP PI = LAP λ = 405 nm $t = 3.1$, 3.5, 3.9 s	PEGDA hydrogel Photoabsorber: Yellow food grade dye	Elastic modulus	Fibroblast	Regionally varied stiffness scaffold by using DLP with different exposure times (3.1, 3.5, and 3.9 s) which affected the mechanical properties of the scaffold, for a 60 % variation in stiffness across the structure (elastic modulus = 17.8 kPa, 22.4 kPa, 30.1 kPa, for each exposure time), maintaining the same architectural geometry.
Dobos et al. (2019) [117]	Not reported	2-PP PI = DAS λ = 722 nm	Gel–NB hydrogel	Crosslinking	L929 mouse fibroblast cells	3D constructs fabricated via 2-PP using Gel–NB hydrogel with sub-micrometer resolution, featureing crosslinking

(*continued on next page*)

Table 2 (*continued*)

Reference (Year)	Tissue	Technique and process parameters	Materials	Type of gradient	Test *in vitro or in vivo*	Main results
		P = 10 – 100 mW t = 70 fs pulses				density gradients and enabling tuned mechanical properties (0.2–0.7 kPa) and enzymatic degradability varying the applied power of the laser. The system supported printing speed up to 1000 mm/s and exhibited uniform cell embedding and distribution, long-term viability, promoted cell adhesion and proliferation.
Gong et al. (2020) [110]	OC	DLP: gelMA PI = LAP λ = UV light P = 30 mW/cm^2 t = 10 s FDM: PCL	Subchondral bone = PCL + HA Cartilage = gelMA + interleukin-4	Radially oriented structure	Mouse fibroblast cells, *in vitro* Rabbit model *in vivo*	Radially oriented scaffold showed cell adhesion and proliferation in a rabbit defect model, *in vivo*. Moreover, the presence of the anti-inflammatory interleukin-4 (IL-4) revealed an anti-inflammatory effect.
Wang et al. (2020) [103]	Bone	SLA PI = Hydroxy cyclohexylphenyl ketone (184) λ = 355 nm Laser intensity = 25 μJ	HA + Di-TMPTA + HDDA	Porosity Mechanical properties	BMSC	Scaffolds with gradient porosity distributed on the horizontal cross-section with different pore sizes. Minimal pore size reached 500 μm with a precision of up to 60 μm. It showed improved cell proliferation of BMSC.
Zhou et al. (2020) [102]	Cartilage	SLA PI = I2959 λ = 355 nm Printing speed = 10 mm/s	GelMA + PEGDA	Composition Compressive modulus	Adipose-serived mesenchymal cells (ADSCs).	Gradient scaffold made of different ratios of gelMA and PEGDA (15 %:10 %, 15 %:15 %, 15 %:20 %, respectively). Inks of different compositions have been fed to the SLA printer. Compressive modulus increased with increasing PEGDA concentrations throughout the scaffold from 1.4 MPa to 3.8 MPa. The gradient scaffold was coated with lysine-functionalized rosette nanotubes (RNTK) a bioactive nanocoating material which is able to improve the chondrogenic differentiation of adipose-derived mesenchymal stem cells (ADSCs).
Schoonraad et al. (2021) [111]	Bone Cartilage	DLP PI = TPO λ = 405 nm t = 6 s	Scaffold structure = PEGDA Bone mimetic hydrogel = PEGNB + HA + TGF-β_3 + BMP-2 Cartilage mimetic hydrogel = PEGNB + TGF-β_3 + BMP-2 Photoabsorber: 2-(2-hydroxyphenyl)-benzotriazole derivative (Tinuvin CarboProtect®)	Structure/ Architecture Porosity Elastic modulus	Bone-marrow derived hMSCs	Scaffold was based on an array of stiff vertical pillars bound by a horizontal lattice structure. Density of the vertical pillars was measured by volume percent, ranging from 6 to 25 % throughout the scaffold with a number of pillars between 45 and 220, respectively. Porosity of the scaffold varied from 94 % to 75 % with the increase of pillars number. The effective modulus was found to increase from 0.5 MPa to 4 MPa. The scaffold induced chondrogenesis and osteogenesis.
Shirzad et al. (2021) [113]	Bone	DLP PI = *H*—Nu-470 λ = UV light	PMMA + chitosan	Structure Elastic modulus	Human osteoblast-like cells (Saos-2)	Scaffolds with gradient architecture made of micro-truss structures. Strut cross-sectional areas decreaed toward the surface (values of cross-sections were 1.3 mm, 0.8 mm, 0.6 mm, 0.55 mm, and 0.3 mm to the inner to outer layers) showing multiple elastic behaviors. Moreover, it was designed by using a modeling tool, the design of experiment approach.
Eckstein et al. (2024) [112]	Cartilage	DLP PI = TPO λ = 405 nm P = 30 mW/cm^2 t = 6 s	Stiff scaffold structure = PEGDA Soft structure = PEGNB hydrogels Photoabsorber: Tinuvin CarboProtect®	Structure Geometry Elastic Modulus	Not evaluated	Scaffolds made of micro-truss structures possessing spatially varied geometry. Diameters of struts were fabricated to vary from 180 μm to 160 μm, providing a gradient in stiffness from 1 MPa to 0.76 MPa.

limitations. The reported structure represented a simplified and conceptual model of the natural osteochondral complex, and not fully captured its native characteristics. Also, even though biocompatibility tests were successfully carried out by using bone marrow stromal cells (MSCs) it served only as a pilot study.

Some years later, Castro et al. developed a novel table-top stereolithography 3D printer aimed at fabricating multi-material, multi-layered structures. Some advantages of this technique included rapid and cost-effective fabrication of complex multilayered constructs. Thus, they produced a porous and highly interconnected three-layered OC graded scaffold (comprising 2 bone layers and 1 cartilage layer) using a mixture of nano-sized HA (nHA), PLGA nanosphere and PEGDA hydrogel [99]. The scaffold contained a gradient in nHA concentration from 10 % to 20 % to mimic the architecture and the mechanical

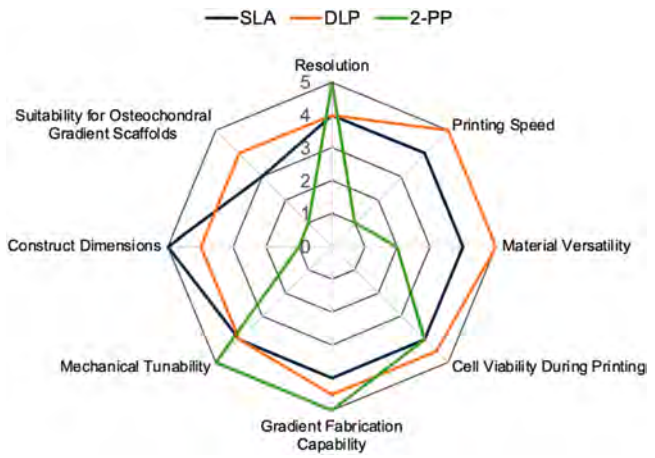

Fig. 5. Qualitative comparison of the strengths and weaknesses of various VPP methods across multiple parameters relevant to osteochondral gradient scaffold fabrication. The scoring (0–5 scale, where 0 = no capability and 5 = very high capability) reflects an aggregated evaluation derived from peer-reviewed scientific studies cited in this review. Parameters assessed include resolution, printing speed, material versatility, cell viability during printing, gradient fabrication capability, mechanical tunability, construct dimensions, and suitability for osteochondral gradient scaffolds.

properties of the subchondral bone layer, and TGF-β1 nanospheres (a growth factor) in the cartilage layer to enhance the osteochondral regeneration. Mechanical tests showed that compressive modulus and elastic modulus were higher in graded scaffolds loaded with nHA (Fig. 6d-i and d-ii). Furthermore, biological tests revealed improved and driven adhesion, proliferation and differentiation of osteochondral hMSCs, particularly due to the presence of gradient growth factor cues [99].

A similar but more sophisticated system, called Multi-Material StereoLithography (MMSL), and based on a bottom-up mask projection approach, was developed by Wu et al. in 2018. By adjusting light power densities, it was possible to fabricate materials with significantly different curing characteristics. In the study, the authors developed three types of multi-resin constructs with various structural features, in which the material changes within layers, between layers, or both. In particular, they fabricated a gradient OC scaffold, made of PEGDA hydrogel and beta-tricalcium phosphate (β-TCP) ceramic suspension to replicate the cartilage and bone tissues, respectively (Fig. 6e) [100]. With this technique, they were also able to obtain a strong interface between the two layers, similar to the one found into the natural OC tissue transition zone. The findings demonstrated that the bond between the hydrogel and the β-TCP ceramic layers was strong enough to resist an applied separation force [100]. However, even though no biological tests were carried out to evaluate biocompatibility of the scaffolds and its efficiency in adhesion, proliferation and differentiation of OC cells, MMSL technique can been considered as one of the best approaches to replicate structural gradient of OC tissue.

Another example of SLA-based scaffold can be found in the studies of Zhou et al. Here, they developed a biomimetic compositional scaffold with two distinct phases: a GelMA-PEGDA-nHA phase mimicking subchondral bone and a GelMA-PEGDA phase loaded with TGF-β1 and PLGA nanoparticles to replicate cartilage tissue (Fig. 6 g) [101]. In the study, hMSCs were cultured in the scaffold, showing successfully induced osteochondrogenic proliferation and differentiation. Expanding on this work, the authors later fabricated a gradient scaffold with different ratios of GelMA and PEGDA (GelMA:PEGDA 15 %:10 %, 15 %:15 %, 15 %:20 %) by feeding the SLA printer with inks of different composition [102]. The result was a scaffold that closely mimicked the compositional, structural and mechanical strengths gradient present in cartilage tissue. Mechanical testing showed that the compressive modulus increased with increasing PEGDA concentrations, with values gradually rising from 1.4 MPa at the top layer to 3.8 MPa at the bottom layer, confirming a gradient in both structure and mechanical properties [102]. As a further step to enhance biological interactions, the authors also performed a surface functionalization of the scaffold, by coating it with lysine-functionalized rosette nanotubes (RNTK), a bioactive nanocoating material which is able to improve the chondrogenic differentiation of adipose-derived mesenchymal stem cells (ADSCs) [102].

The most recent study involving SLA printing was conducted by Wang et al. They designed HA cylindric scaffolds with a gradient porosity distributed on their horizontal cross-sections, featuring varying pore sizes, as shown in Fig. 6f. This study highlighted the high resolution achievable with SLA technique: the minimum pore size reached 500 μm with a precision of up to 60 μm, while the maximum pore size was about 3 mm; on the other hand, the porosity gradient was measured, with a variation of total porosity from 9.2 % to 94.6 % along the radius of the scaffold [103]. The evident pore size and porosity variations throughout the scaffold also affected its mechanical properties. Compression tests showed that the scaffolds had a compressive strength varying from 5.6 MPa to 18.4 MPa and an elastic modulus ranging from 2.4 GPa to 5.9 GPa, effectively replicating the gradient mechanical properties and functional performances of natural bone. Moreover, bone marrow mesenchymal stem cells (BMSCs) were cultured within the scaffold, showing enhanced cell proliferation. Notably, the regions with higher porosity supported improved cell proliferation, underscoring the biological advantages of the scaffold's design. However, *in-vitro* experiments were at the preliminary stage and more detailed data were required to have a better evaluation about osteogenic properties [103].

3.2. *Digital light processing (DLP)*

Similar to SLA, the DLP process also involves the design of a 3D object with CAD software and a tank to hold the photopolymerizable liquid resin. DLP technology was invented in 1987 by Dr. Larry Hornbeck of Texas Instruments, and it was initially used in digital projectors before being adapted for 3D printing. DLP's 3D printing application, however, became prominent in the 1990s and early 2000s, when it began being applied for resin printing, and has continued to evolve to the present day [104]. The choice between SLA and DLP depends on the specific use case. The most important difference between DLP and SLA technologies lies in their light sources, as illustrated in Fig. 3e. Unlike SLA, which employs a laser to cure the resin point by point, DLP utilizes digital micromirror devices (DMD), which consist of a large array of microscopic mirrors arranged in a grid. These mirrors can be individually tilted to be in an "on" or "off" position, allowing them to reflect light and project an image. Each mirror corresponds to one or more pixels in the projected image. When the micromirrors are in the "on" position and are struck by light, they reflect it to produce an image. Conversely, micromirrors in the "off" positions are oriented to block the light, creating dark areas. When the light reflected by DMD mirrors is directed toward the resin, it is selectively illuminated and polymerized an entire layer at once, resulting in a solidified material with the same shape as the projected image. This layer-by-layer curing approach enables DLP to achieve faster print speeds compared to SLA while maintaining high resolution [92].

One of the first studies on DLP-based OC gradient scaffold was conducted by Chen et al. in 2019, who used a DPL variant, the desktop-SLA, to fabricate high resolved 3D scaffolds for OC repair [105]. The researchers made scaffolds by mixing decellularized cartilage ECM, GelMA hydrogels and MSC-derived exosomes, developing an architecture with radially oriented channels in which a more efficient exchange of nutrients and waste was possible, promoting improved cells and tissues ingrowth, ECM deposition, and cell interaction (Fig. 7a) [106–108]. The study demonstrated that the pore size of the scaffold varied depending on the concentration of ECM used in the hydrogel mix, ranging from 91.6 μm ± 7.0 μm to 106.8 μm ± 6.9 μm. Additionally, the

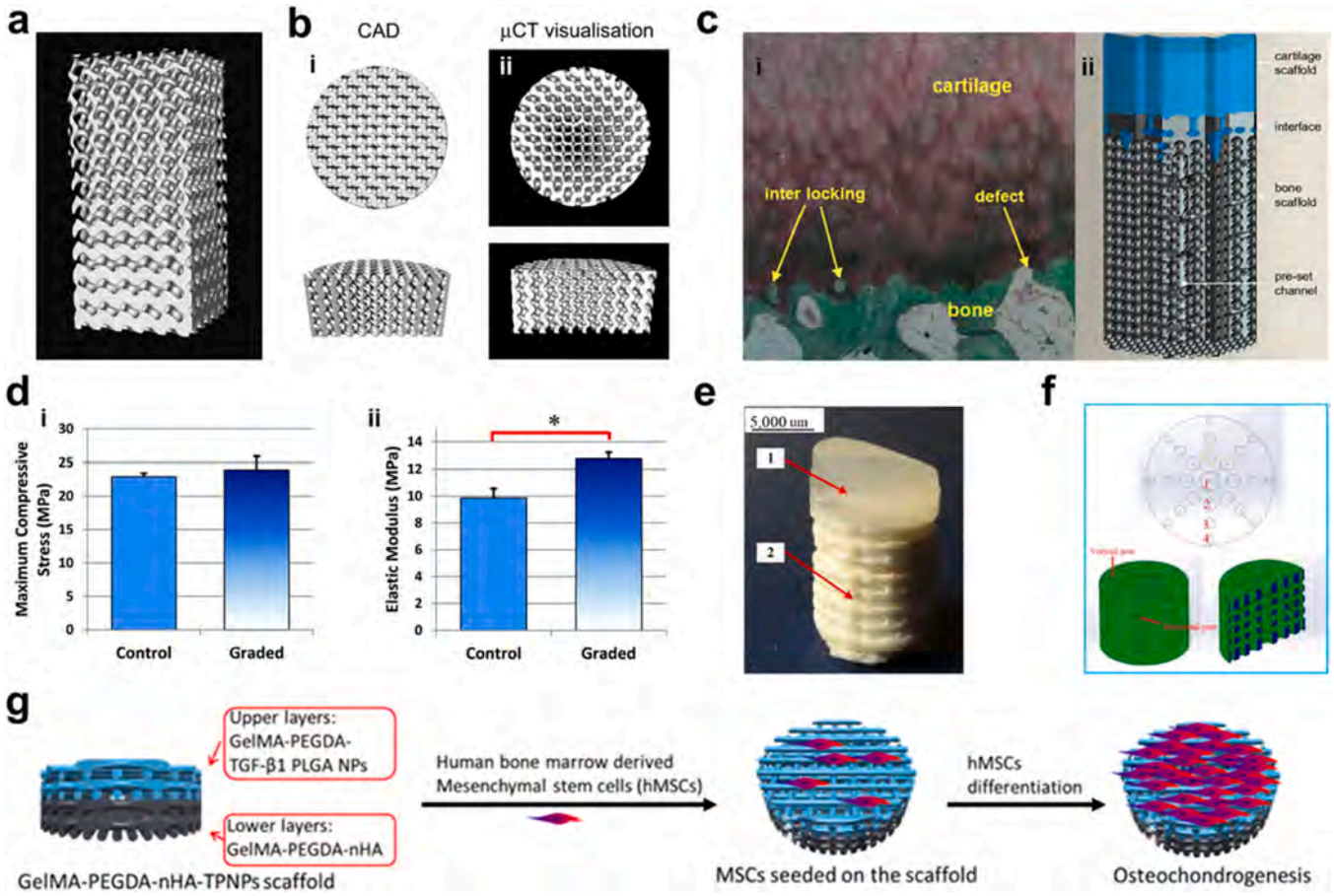

Fig. 6. OC gradient scaffolds obtained by SLA technique. a) Micro-computed tomography (µCT) of the PDLLA-made OC scaffold: the structure shows a gyroid architecture with a gradient in porosity and pore size. Reproduced and adapted with permission from Ref. [95]. Copyright 2010, Elsevier. b)-i top-view and cross-section of computer-aided designs (CAD) image of the modeled PDLLA scaffold with gyroid pores; b)-ii top-view and cross-section of µCT visualization of the same scaffold fabricated with SLA, showing that the scaffold design is very accurately reproduced. Reproduced and adapted with permission from Ref. [96]. Copyright 2011, Elsevier. c)-i Image obtained by histological analysis of OC tissue that shows transitional structures between the bone and cartilage layers; c)-ii schematics of cross-section of the scaffold (made of acrylamide matrix loaded with β-tricalcium phosphate (β-TCP)) mimicking cartilage and bone layers and the transitional interface. Reproduced and adapted with permission from Ref. [98]. Copyright 2012, Emerald Group Publishing. d) Mechanical tests carried out on gradient OC scaffold (made of PLGA/PEGDA and loaded with nHA) and control without nHA: d)-i a few increase in compressive modulus is observed in the graded OC scaffold compared to non-nHA control; d)-ii An increase of 29 % in elastic modulus is observed in the graded OC scaffold compared to non-nHA control (Data are mean ± StdEM, $n = 5$, $^*p < 0.05$). Reproduced and adapted with permission from Ref. [99]. Copyright 2015, Royal Society of Chemistry. e) Picture of scaffold made of **1** PEGDA hydrogel and **2** β-TCP obtained by multi-material mask projection stereolithography (MMSL). Reproduced and adapted with permission from Ref. [100]. Copyright 2018, Emerald Group Publishing. f) Schematics of a 3D scaffold model made by the software Solidworks. The OC scaffold made of HA shows gradient porosity distributed on horizontal cross-section with different pore sizes. Reproduced and adapted with permission from Ref. [103]. Copyright 2020, Elsevier. g) Schematics of a compositional gradient scaffold made of two mainly phases of gelMA-PEGDA-nHA and gelMA-PEGDA loaded with TGF-β1 and PLGA nanoparticles mimicking the structure of subchondral bone and cartilage tissues; the mesenchymal stem cells are seeded and cultured in the scaffold showing successfully induced osteochondrogenic proliferation and differentiation. Reproduced and adapted with permission from Ref. [101]. Copyright 2019, Elsevier.

Young's modulus increased with higher ECM concentrations, from 16.09 kPa ± 0.56 kPa to 37.72 kPa ± 2.82 kPa, indicating that the scaffold became stiffer with higher ECM content. Furthermore, the researchers proved that these scaffolds can promote cartilage regeneration by restoring cartilage mitochondrial dysfunction and enhancing chondrocyte migration [105].

Another approach to building OC gradient scaffold is reported by Xue et al. They fabricated a PEGDA-based hydrogel scaffold with regionally varied stiffness by using DLP, adjusting exposure times (3.1, 3.5, and 3.9 s) to influence the mechanical properties of the scaffold. Mechanical tests demonstrated the feasibility and effectiveness of the used approach showing that with longer exposure times, which lead to higher cross-linking degree of the printed hydrogel, stress increased while strain decreased. In particular, the elastic modulus had a 60 % variation across the structure, with values of 17.8 kPa, 22.4 kPa, and 30.1 kPa for each respective exposure time, while maintaining the same architectural geometry (Fig. 7b) [109]. This study contributed to the field by highlighting the role of mechanical property gradients in tissue regeneration, particularly in bone and cartilage.

Over the past five years, the combination of VPP with other AM techniques has become a prevalent strategy to create composite scaffolds and decoupling the mechanical and biochemical needs to improve performances. Gong et al. exploited this approach by integrating two different types of AM techniques to fabricate osteochondral scaffolds with layers of different architectures [110]. They used FDM technique to print the porous PCL-HA lower layer to mimic the subchondral bone zone, and DLP one to print the radially oriented GelMA upper layer to simulate the cartilage layer (Fig. 7c-i and iii). In this study, the PCL-HA layer showed the highest porosity (~70 %), essential for bone regeneration, while the GelMA part had lower porosity, still maintaining a gradient porosity throughout the structure. In an *in vivo* rabbit defect model, both layers demonstrated good cell adhesion and proliferation (Fig. 7c-ii). In addition, the lower layer promoted osteogenic differentiation, while the upper layer revealed an anti-inflammatory effect due

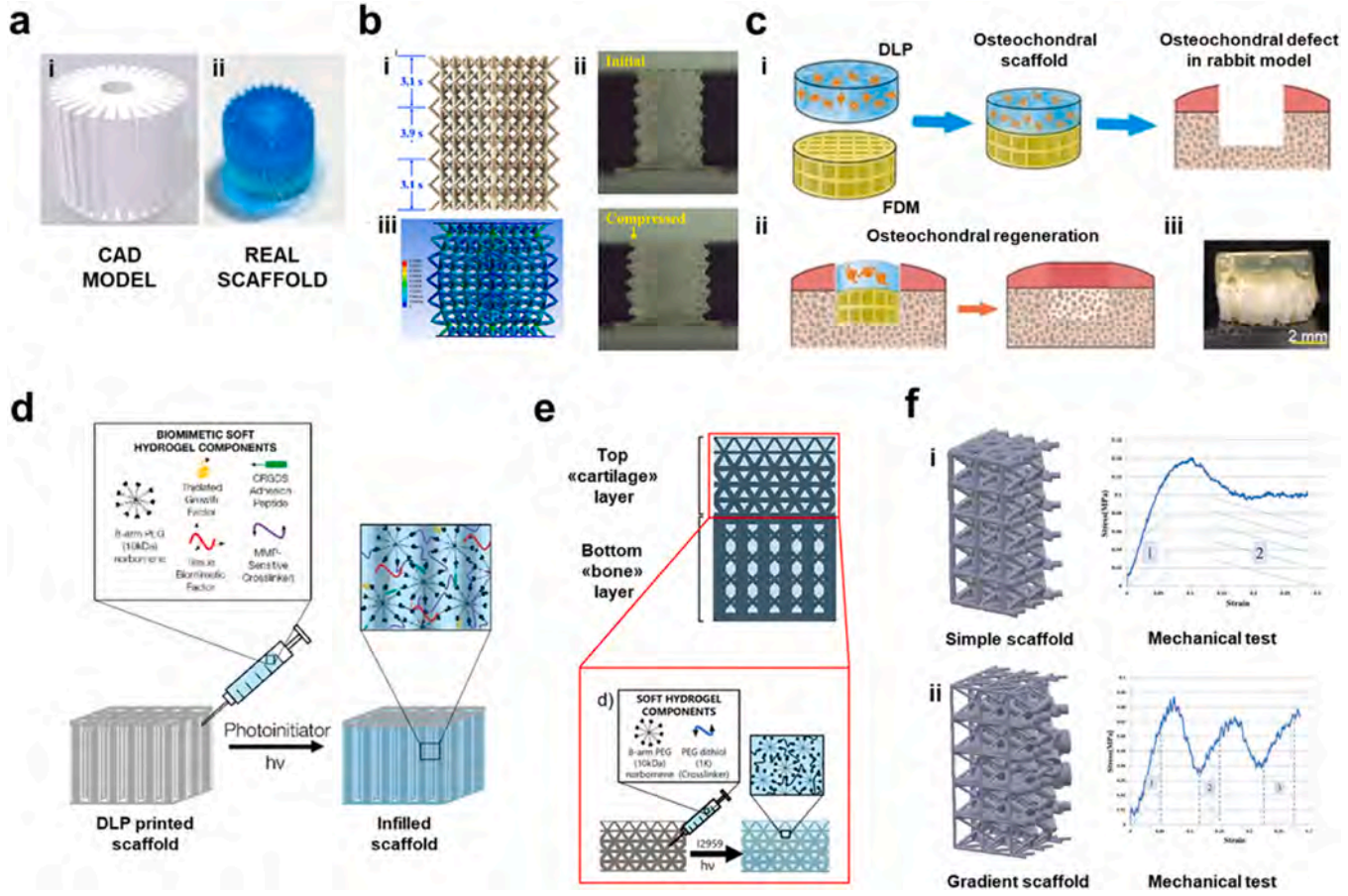

Fig. 7. OC gradient scaffolds obtained by DLP printing technique. a)-i CAD image of an OC gradient scaffold with radially oriented channels; a)-ii real picture of the previous scaffold made of decellularized ECM, gelMA hydrogel and loaded with MSC-derived exosomes (stained with methylene blue dye). Reproduced and adapted with permission from Ref. [105]. Copyright 2019, Ivyspring International Publisher. b)-i example of a 3D model scaffold obtained with different exposure times during the printing process (reported on the left); b)-ii pictures of the scaffold before and after compression test; b)-iii simulated strain model obtained by the compression of the scaffold. Reproduced and adapted with permission from Ref. [109]. Copyright 2019, American Chemical Society. c)-i combination of FMD and DLP techniques to print the porous PCL-HA lower layer to mimic the subchondral zone and the radially oriented gelMA upper layer to simulate the cartilage layer, respectively; c)-ii integration of the scaffold into an OC defect of a rabbit model and regeneration of the tissue; c)-iii real picture of the scaffold. Reproduced and adapted with permission from Ref. [110]. Copyright 2020, Elsevier. d) schematics of a scaffold made of an array of stiff vertical pillars printed by DLP, whose density is varied throughout the structure to provide different stiffness values and infilling of the structure with soft hydrogel precursor solution followed by photopolymerization. Reproduced and adapted with permission from Ref. [111]. Copyright 2021, IOPScience Publishing. e) schematics of a micro-truss structured scaffold printed by DLP and infilling of the structure with hydrogel precursor and photopolymerization. Reproduced and adapted with permission from Ref. [112]. Copyright 2024, Springer Link. f) CAD images and mechanical tests (compressive stress-strain curves) of the f)-i simple monolithic scaffold and f)-ii gradient scaffold that show different mechanical behaviours: the simple scaffold demonstrates a classic behaviour in which the plastic region (**2**) follows the linear elastic trend (**1**), meanwhile the gradient scaffold shows multiple elastic behaviors under compressive load. Reproduced and adapted with permission from Ref. [113]. Copyright 2021, Elsevier.

to the presence of the anti-inflammatory interleukin-4 (IL-4) loaded into the GelMA [110].

Schoonraad et al. also combined two different methods to develop a mechanically supportive and cell-instructive system composed of PEGDA and PEGNB hydrogels, respectively [111]. The authors decoupled the required mechanical and biochemical components by designing an OC scaffold printed by DLP. The scaffold featured an array of stiff vertical pillars bound by a horizontal lattice structure, whose density was varied throughout the structure to provide different stiffness levels without requiring multiple resin formulations (Fig. 7d). To enhance biological functionality, the scaffold was subsequently infused with MSCs and biomimetic soft hydrogels composed of functionalized and HA-loaded PEG formulations, able to mimic the cartilage and bone layers, respectively (Fig. 7d) [111]. In particular, the density of the vertical pillars, measured as a volume percentage in the 3D printed structure, ranged from 6 to 25 % across the scaffold, with the number of pillars varying between 45 and 220. As the pillar density increased, scaffold porosity decreased from 94 % to 75 %, while the effective modulus rose from 0.5 MPa to 4 MPa. Finally, the study demonstrated that the scaffold successfully induced both chondrogenesis and osteogenesis [111].

More recently, Eckstein *et al.* designed and developed scaffolds with gradients in geometry and stiffness using PEGDA to mimic the mechanical properties of cartilage tissue, by employing a novel and customized DLP technique [112]. Specifically, a custom projection microstereolithography (μSLA) system was utilized, capable of producing structures with unprecedented resolution of 1 μm – 10 μm. In this work, the authors designed and fabricated unique micro-truss structures with spatially varied geometry and controlled stiffness gradients. Diameters of struts were fabricated to vary from 180 μm to 160 μm, providing a gradient in stiffness from 1 MPa to 0.76 MPa. Then, they infused the scaffold with soft PEGNB hydrogel which also incorporates biochemical cues to support osteogenic and chondrogenic differentiation (Fig. 7e) [112].

Shirzad et al. fabricated scaffolds with architectural and mechanical property gradients using chitosan-coated PMMA, by employing the DLP technique [113]. The gradient in the scaffold was achieved by varying the strut cross-sectional areas, which gradually decreased toward the

surface. Specifically, cross-sectional values ranged from 1.3 mm in the inner layers to 0.3 mm in the outer layers (intermediate values: 0.8 mm, 0.6 mm, and 0.55 mm). This reduction in cross-sectional area resulted in a more complex mechanical response with respect to simple scaffolds. Indeed, the authors compared physical, mechanical, and biological properties of the gradient scaffold with a monolithic one that had the same porosity but a uniform structure. Mechanical testing revealed that gradient scaffolds exhibited multiple elastic behaviors under high compressive load, identified as elastic areas number 1, 2 and 3 in Fig. 7f-ii. In contrast, monolithic scaffolds showed a single elastic behavior (Fig. 7f-i). This behavior closely mimics the mechanical properties of natural bone tissue. However, biological tests using human osteoblast-like cells (Saos-2) showed no significant differences in cell adhesion between the two scaffold types, as adhesion was primarily influenced by the chitosan coating. In addition, to optimize the fabrication process and achieve the desired properties of the scaffolds, the researchers employed a statistical model, specifically the Response Surface Methodology (RSM) [113]. RSM is a DoE approach useful for modeling complex systems in which desirable characteristics are interdependent and influence one another [114]. Notably, in their study, the researchers aimed to identify the optimal truss-like scaffold structure with the highest porosity and modulus values, utilizing a polynomial model within the RSM technique, which effectively considers the interactive influences of multiple variables. Their results demonstrated that the RSM technique enables to improve the mechanical and physical properties of scaffolds while keeping costs low.

3.3. 2-Photon polymerization (2-PP)

In contrast to SLA and DLP, which typically relies on the absorption of a single photon by individual molecules to initiate crosslinking reactions, 2-PP technique is a type of multi-photon polymerization (M-PP) where simultaneous absorption of two low-energy photons by one atom or molecule occurs, allowing it to be excited to a higher energy state (Fig. 3f). The absorption of photons in the near-infrared (NIR) spectrum triggers photopolymerization and, thus, the solidification of the liquid material only where the light intensity is the highest also known as the focal point. The focal point is moved by galvo scanners in the focal plane at speeds of hundreds of millimeters per second and the laser beam is focused into the photosensitive resin using a high numerical aperture objective lens. By precisely controlling the position of the focal point in three dimensions, complex 3D structures with features on the nanometer scale can be created [2]. Similar to other AM techniques, 2-PP builds objects layer by layer, polymerizing the entire volume of each layer at once. However, the time required to fabricate scaffolds of a physiologically relevant size using 2-PP makes it often an impractical option.

To date, only a limited number of studies in literature report promising materials and structures printable by 2PP and potentially suitable for biomimetic gradient tissue engineering, but none of them concern the fabrication of OC gradient scaffolds. However, some of these studies are included in this review as they either present photopolymers with tunable mechanical properties that, although currently used in monolayer constructs, hold clear potential for future application in OC gradient scaffold fabrication, or demonstrate gradient scaffold strategies applied to other tissues, offering transferable design principles.

In 2020 Weisgrab et al. overcame limitations related to slow fabrication speeds of 2-PP, which typically restrict the achievable scaffold size, by optimizing a highly reactive poly(trimethylene-carbonate (PTMC)-based photopolymer and refining printing parameters. The scaffolds were designed using a buckyball-based repeating unit, obtaining large and highly porous biodegradable structure exhibiting a porosity of 96 %, with fine struts around 20 μm – 30 μm in thickness. Mechanical properties were also influenced by the scaffold's microarchitecture, ensuring structural integrity that remains retained even throughout 28 days of cell culture, while maintaining also flexibility. The study evaluated cell adhesion, proliferation, and differentiation into osteogenic and chondrogenic lineages using various methods and different types of cells, confirming that cells adhered to the scaffolds, proliferated over time, and remained viable. They successfully differentiated into cartilage and bone-like tissue, demonstrating the scaffold's suitability for tissue engineering applications [115].

In 2022 Hauptmann et al. developed a photosensitive copolymer system, D,L-lactide-ε-caprolactone as tunable material scaffold for 2-PP, to replicate the complex 3D architecture of the osteochondral ECM for bone and cartilage reconstruction. Employment of 2-PP technology allowed to fabricate highly precise and complex structures, such as cuboids with dimensions in the range of 83 μm - 175 μm By changing the ratio of alanine:ε-caprolactone (20:80, 40:60, 60:40 and 80:20) to fine-tune the mechanical and degradation properties, they found that increasing the alanine content the stiffness of the final scaffold reduced, while the copolymer wettability and degradation rate simultaneously enhanced. Precisely, the study reports that for alanine:ε-caprolactone 20:80 the stiffness is around 400 kPa, while for alanine:ε-caprolactone 40:60, the stiffness is approximately 230 kPa, matching in principle the stiffness of OC tissue showing good suitability for osteochondral reconstruction [116].

Instead, Dobos *et al.* explored the application of gelatin–norbornene (Gel–NB) hydrogels as bioinks for high-definition two-photon polymerization (2PP) bioprinting. They fabricated 3D constructs, having sub-micrometer resolution and a crosslinking density gradient, with direct embedding cells into them via 2-PP. Then, characterized the structures and characterized 3D constructs having sub-micrometer resolution and a crosslinking density gradient. The authors demonstrated that the highly reactive thiol-ene system supports fast printing speeds (up to 1000 mm/s) and allows tuning of hydrogel mechanical properties (0.2 kPa – 0.7 kPa) and enzymatic degradability varying the applied power of the laser. Moreover, three-week cell culture studies proved that the printed constructs exhibit excellent biocompatibility, support long-term cell viability, adhesion, and proliferation, and allow for uniform cell distribution independent of scaffold pore size. Therefore, these results position Gel–NB-based 2-PP bioprinting as a powerful platform for fabricating complex, cell-laden 3D microenvironments and offer a compelling perspective on integrating precise structural control, embedding living cells, and maintaining high cell viability in gradient scaffolds that effectively mimic the heterogeneity of native tissues [117].

Even though some limitations in producing scaffolds for OC tissue with 2-PP have been addressed, such as the possibility to obtain large structure with high resolution, producing scaffolds with adequate topographical control on a nano and micro scale and continuous material gradients remains time-consuming, limiting its practicality for large-scale tissue engineering [118,119]. Additionally, the limited availability of biocompatible and biodegradable photopolymers restricts the range of materials that can be used to create mechanically robust and biologically functional gradient structures [120]. Another challenge lies in integrating different material properties within a single scaffold to mimic the gradual transition from cartilage to bone since 2-PP typically relies on a single resin formulation, even if recent studies are increasingly exploring combinations of various resins [121]. Future advancements in multi-material printing, faster processing speeds, and improved bioresins will be necessary to overcome these limitations and make 2-PP a viable option for large-scale gradient osteochondral scaffold production [2].

4. Precursor materials for fabrication of OC scaffolds by VPP

4.1. Formulation of photopolymer resins for OC scaffolds

Resins used for OC scaffold fabrication typically consist of three main components: the matrix, the photo-initiator, and the filler. The matrix provides the structural framework of the final scaffold and is composed of monomers or oligomers from natural or synthetic sources that can

photo-polymerize and cure in the presence of a photo-initiator. The choice between natural and synthetic materials depends on their intrinsic properties, which ultimately influence the scaffold's characteristics. Unlike natural polymers, synthetic polymers offer tunable mechanical properties, degradation rates, and viscosities, which can be adjusted by modifying their chemical structure and molecular weight. However, synthetic polymers generally exhibit lower biocompatibility, particularly in terms of cell adhesion and viability [2].

Natural polymers are extensively used in biomedical applications due to their biocompatibility, ease of processing, and controlled degradation kinetics. They help minimize implant cytotoxicity closely resembling the ECM. A common strategy to make them photo-crosslinkable involves their functionalization with reactive groups, such as acrylates or thiol-ene components, allowing for photoinduced polymerization in the presence of specific photo-initiators. Among natural polymers, photocross linkable hydrogels are the most commonly used in VPP technologies due to their biocompatibility, hydrophilic nature, mechanical and biological properties, and the ease of curing under light exposure [48].

The most frequently used hydrogel in OC gradient scaffold fabrication is GelMA, a biocompatible material derived from gelatin functionalized with methacrylic moieties. Due to its methacrylic functional groups, GelMA undergoes photo-crosslinking and solidification under light irradiation via SLA or DLP techniques. Gelatin itself can also be employed to produce OC scaffolds. Gelatin is obtained from collagen, the most abundant protein naturally present in the ECM of OC cells and is widely used in several biomedical applications. Due to their inherently soft nature, gelatin and GelMA are often combined with inorganic fillers such as β-TCP, which is usually cured with SLA technique [98]. However, the mechanical strength of natural polymers is generally insufficient for load-bearing applications, which is a critical requirement in OC scaffolds. Additionally, natural polymers can exhibit batch-to-batch variability, potentially affecting the consistency of scaffold properties [122]. Thus, natural polymers are often combined with other synthetic polymers that exhibit enhanced mechanical properties and also can be synthesized in controllable processes and on a large scale.

Synthetic polymers offer tunable mechanical properties and degradation rates. Polyethylene glycol diacrylate (PEGDA), for instance, is a PEG derivative functionalized with diacrylates moieties and is highly photoreactive, enabling the fabrication of scaffolds with precise and complex architectures through VPP techniques. However, synthetic polymers often lack bioactive sites necessary for effective cell adhesion and may produce acidic degradation byproducts that could lead to inflammation. Their hydrophobic nature can further hinder cell attachment and proliferation [123].

PEG can be further functionalized with norbornenes functional groups giving PEGNB, which is capable of photo-crosslinking *via* SLA and DLP techniques, giving OC scaffolds with high mechanical properties [111]. However, the bioinert nature of PEG-based polymers often results in low cell adhesion, limiting their biomedical applications. For these reasons, PEGDA and PEGNB are often blended with natural polymers [111].

Polyesters such as poly-d-lactic acid (PDLA), poly-l-lactic acid (PLLA), polycaprolactone (PCL), and poly(lactic-co-glycolic acid) (PLGA) are also commonly used in OC scaffold fabrication due to their biodegradability, biocompatibility, and mechanical properties that support tissue regeneration. They can be properly functionalized with methacrylic groups enabling them to undergo photo-polymerization and photo-crosslinking via SLA and DLP technologies [87,88,92,101,108,109].

However, to harness the benefits of both material types, composite scaffolds combining natural and synthetic polymers have been developed. For example, integrating GelMA with PEGDA has resulted in scaffolds that show enhanced mechanical properties while maintaining favorable biocompatibility. Studies have demonstrated that GelMA/PEGDA hydrogels possess increased mechanical strength compared to pure GelMA hydrogels, along with suitable degradation rates and support for osteoblast adhesion and proliferation [124–126].

Another crucial component of the OC resin is the photoinitiator (PI), which is necessary to initiate the reaction upon light irradiation. The choice of the wavelength to depends on the absorption peak of the selected PI [48]. The working mechanism through which the reaction occurs is also driven by PI. Three main crosslinking processes are usually described in the literature: free radical polymerization, step-growth reaction, and photomediated redox polymerization [127].

One of the most used PIs is 2-hydroxy-1-[4-(2-hydroxyethoxy) phenyl]−2-methyl-1-propanone, better known as Irgacure 2959 or I2959 [101,102,111]. It is often used in water-based resins or hydrogels in combination with GelMA, PEGDA or PEGNB [101,102,111]. However, low water solubility, low polymerization efficiency and cytotoxicity at high concentrations are the main drawbacks of I2959 [128]. Some of these limitations can be mitigated by replacing I2959 with bis (2,4,6-trimethylbenzoyl)-phenylphosphine oxide (BAPO), which offers higher solubility and polymerization efficiency [48,99,128,129]. Nevertheless, BAPO can also inhibit cell growth and induce apoptosis [130]. Another effective water-soluble PI is lithium phenyl-2,4,6-trimethyl benzoyl phosphinate (LAP), which exhibits low cytotoxicity, maintaining cell viability above 80 % at low concentrations. In contrast, 2,4,6-trimethyl benzoyl diphenylphosphine oxide (TPO) has low water solubility but is considered the most efficient PI for nonaqueous systems due to its high polymerization rate and good cytocompatibility. However, given the importance of developing water-soluble PIs, many researchers are currently exploring chemical modifications of both TPO and BAPO to incorporate functional groups that enhance their solubility in aqueous environments [131,132].

To enhance the bioactivity of synthetic polymers and improve the stiffness and compressive strength of natural polymers, composites of polymers with inorganic materials are obtained by introducing bioceramics, such as HA and β-TCP. Also materials like whitlockite, bredigite, and bioactive glass are often combined with polymer matrices in scaffolds, improving degradation behavior and biological responses [47–49]. Since native OC tissue is naturally composed of different components, achieving an accurate biomimetic structure requires the combination of both stiff and soft materials [98–101,103,110].

Furthermore, diluents are often added to reduce the viscosity of the resin filled in the tank of the SLA or DLP instrument, ensuring proper printing [133]. For example, water is used when hydrogels like GelMA and PEGDA serve as matrices, but also non-reactive organic solvents, such as NMP or ethyl-lactate, are often employed with more apolar polymers [95,102,133]. Even inhibitors, dyes, and dispersants are frequently included in the formulation to prevent premature cross-linking, enhance light absorption, and improve the filler distribution, respectively, giving homogeneous liquid resins [48,95,97,133]. For example, radical scavengers are inhibitors molecules able to remove or de-activate impurities and avoid undesired reaction products. They help control the surface polymerization process, reducing premature cross-linking and enabling better surface definition. One of the most used in the fabrication of OC scaffolds is α-tocopherol, commonly known as vitamin E, due to its good antioxidant activity, regeneration mechanisms, chemical reactivity and biocompatibility [95,96,134,135]. On the other hand, photoabsorbers also play an important role when high quality printability and high resolution are requested. They are usually dyes and help manage the light absorption and distribution and ensure precise curing, which is particularly important for printing intricate and high-resolution geometries. Indeed, the presence of photoabsorbers limits the deep penetration of light into the resin, avoiding curing of unintended areas which leads to over-polymerization. Some of them are successfully used in the fabrication of gradient OC scaffolds when visible light is used as source. In order to control the cure depth, Orasol Orange G dye, belonging to the azo-dye family, was employed in the works of Melchels et al. [95,96,136]. It has a moderate biocompatibility and absorbs light in the range of 400–500 nm. Yellow food grade dye has

been utilized by Xue *et al.* to mitigate light dispersion and optimize printing resolution [109,136]. It is often a natural dye, absorbing light in the range of 350–450 nm with a good biocompatibility. On the other hand, when UV light is used, UV blockers or UV absorber can be utilized for the same reason, but with limited biocompatibily [2]. An example is Tinuvin Carboprotect, utilized in the works of Shoonraad et al. and Eckstein et al., a benzotriazole derivative [111,112,136]. Inhibitors and photoabsorbers used in the fabrication of OC scaffolds are also reported in Table 2.

In most cases, post-treatments are required to ensure that 3D printed scaffolds achieve the desired mechanical properties, surface quality, and biological functionality. After the printing process, steps like post-curing with UV light or thermal treatments may be necessary to fully polymerize the material by increasing the final cross-linking density and the degree of polymerization [137]. These processes enhance mechanical properties, increasing the long-term structural stability of the printed structure [137]. Washing with alcoholic solvents (*e.g.* ethanol, isopropanol) is usually employed to remove residual non-polymerized resin and improve the surface finish [138]. At the same time, biological functionality is usually improved by surface treatments and functionalization of the scaffolds with bioactive factors.

Anyway, the formulation of the photocurable bioinks for scaffold production remains a primary concern, as it is inherently guided by the need to achieve an optimal compromise between a resin that fulfils the requirements for scaffold fabrication via VPP and one that results in a matrix with adequate mechanical properties, stability under physiological conditions, and the capacity to promote osteogenesis and chondrogenesis. In this regard, it is important to note that, while the scaffolds for osteochondral (OC) regeneration produced via VPP have been extensively characterized in terms of mechanical behaviour and stem cell response, they have not been thoroughly evaluated for their stability to sterilization, which is mandatory for their intended purpose. Additionally, their degradation rate under *in vitro* physiological and *in vivo* conditions has not been comprehensively assessed. Biological studies conducted in combination with the cell component, that can provide indirect insights into scaffold stability in the physiological environment, are generally limited to a few weeks. As a result, these studies do not provide any data on the long-term stability of these materials, nor on their stability to sterilization, both of which are crucial considerations for their practical application.

4.2. Bioactive factors for surface functionalization of OC scaffolds

Matrix, photoinitiator, and fillers serve as key constituents in the fabrication of gradient OC scaffolds via vat polymerization techniques. They play an essential role in accurately replicating the gradient structure and the mechanical properties of the native OC tissue. Post-curing treatments are crucial for optimizing the scaffold performance, especially for applications in tissue engineering and biomedical implants, where precise control over the material properties is critical for successful outcomes. Additionally, both surface functionalization and the incorporation of bioactive molecules within the scaffold bulk are vital for promoting OC tissue regeneration [139].

Surface functionalization usually involves physical or chemical modifications of the outer layer of the scaffold to enhance specific cellular responses. For instance, plasma treatment can be used to activate the scaffold surface, improving hydrophilicity and facilitating the attachment of bioactive molecules that promote cell adhesion. Biomimetic surface coatings, such as collagen and hyaluronic acid, can further mimic the natural extracellular matrix and enhance cell-scaffold interactions [7,25,140,141]. In a recent work, Shirzard et al. modified the surface of a PMMA scaffold for bone repair, fabricated using the DLP technique, with a chitosan coating to promote and evaluate the adhesion of human osteoblast-like cells (Saos-2) [113].

The scaffold surface can also be functionalized with various chemical groups or bioactive cues, such as peptide sequences, to enhance growth and chondrogenic differentiation [102]. For example, Zhou et al. chemically modified the surface of a gradient GelMA-PEGDA scaffold using rosette nanotubes, a class of self-assembly nanobiomaterials composed of DNA-based analogues functionalized with lysine (RNTK). Compared to control scaffolds, this construct significantly enhanced cell proliferation and the synthesis of GAG, collagen II, and total collagen, highlighting its potential to promote chondrogenic differentiation and establishing it as a promising candidate for cartilage repair and regeneration [102].

Another important class of peptides is represented by growth factors. They can regulate tissue development, regeneration, and homeostasis [99,101,111]. Members of the transforming growth factor-β (TGF-β) and bone morphogenetic proteins (BMPs) families have gained attention for their role in bone and cartilage repair. TGF-β_1, TGF-β_3 and BMP-2 are commonly incorporated into complex liquid resin and printed together with the matrix *via* SLA and DLP techniques to create biomimetic OC scaffolds [99,101,111].

5. AI-driven optimization in design and fabrication of OC scaffolds by VPP

The convergence of artificial intelligence (AI) and advanced biomaterial design is driving a new era of innovations in the field of osteochondral tissue regeneration, particularly in the optimization of gradient scaffolds. Recent literature underscores the transformative potential of AI-driven approaches in analysis and understanding of the complex relationships among the key biological, chemical, and mechanical factors crucial for successful osteochondral tissues repair [142–150]. Machine learning algorithms, such as neural networks and support vector machines, and genetic algorithms are increasingly employed to analyze big datasets encompassing material composition, fabrication parameters, and cellular responses. This enables the creation of predictive and descriptive models and the prediction of optimal scaffold architectures that mimic the native osteochondral tissue's intricate gradient structure, where cartilage transitions seamlessly into subchondral bone [151–153].

However, while AI-methods are predominantly applied to extrusion-based 3D printing technologies, their use in VPP technologies remains rare. For instance, Huang *et al.* used a Shape Deviation Generator (SDG) framework, leveraging a convolution-based approach, to enhance 3D printing accuracy of a SLA process. In particular, their primary aim was to establish a data-analytical method for predicting and compensating for 3D shape deviations by accurately modeling the layer-by-layer fabrication process. The conclusion highlighted that the SDG allowed to obtain a consistent description of 3D shape formation, effectively separating error sources, and yielding valuable process insights. This research paves the way for improved geometric accuracy in SLA through advanced machine learning techniques, though further work is needed to extend its application to complex geometries [154].

Instead, Xu *et al.* used a machine learning algorithm to address the critical challenge of UV irradiation-induced cell damage in SLA-based bioprinting. By analyzing the impact of key process parameters (UV intensity, UV exposure time, GelMA concentration, and layer thickness) the authors successfully built a model demonstrating high predictive accuracy, achieving an R^2 of 0.953, of the cell viability under varying SLA bioprinting conditions. The conclusion emphasized the model's ability to quantify the significance of each parameter, revealing UV exposure time as the most influential, and highlighted the potential of machine learning to overcome limitations of physics-based models in predicting cell viability. However, other bioprinting parameters which may affect cell viability such as GelMA degree of functionalization, photoinitiator type and concentration, and post-printing incubation time should be taken into account for a more comprehensive analysis [155].

Overall, computational methods for scaffold design emerge as powerful designing tools able to surpass traditional fabrication

limitations, leading to production of constructs with unprecedented precision and efficiency, and offer a versatile toolkit for accelerating the discovery of optimal gradient structures.

6. Conclusions, current challenges and future perspectives

6.1. Conclusions

OC tissue damage, caused by structural defects, infections, and degenerative diseases, remains a major challenge in regenerative medicine. Over the years, numerous surgical strategies have been developed for OC tissue repair. However, these approaches are often invasive, with risks of infection, immune responses, and prolonged recovery times. Consequently, tissue engineering has emerged as a promising alternative, aiming to design biomimetic scaffolds that replicate the structure and function of native OC tissue, promoting cell attachment, proliferation, and new tissue formation.

A critical aspect of recreating the complex structure of OC tissue is replicating the mechanical and physicochemical characteristics of its various layers and interfaces. Currently, continuous gradient OC scaffolds, which gradually change characteristics such as chemical composition, geometry, density, porosity, and mechanical properties within the same structure, without forming discrete layers, are considered the most effective ones in mimicking the complex structure of OC tissue. This approach also enables the customization of scaffold geometry to meet patient-specific requirements and applications.

Among AM technologies for tissue engineering constructs, vat photopolymerization techniques, including SLA and DLP, have demonstrated superior precision and control, making them ideal for fabricating gradient OC scaffolds. Compared to traditional AM methods such as FDM and SLS, VPP enables higher resolution, smoother surface finishes, and tunable mechanical properties while minimizing material waste.

This review highlighted the advancements in SLA and DLP for gradient scaffold fabrication, summarizing key studies and identifying novel design strategies, material formulations, and optimization techniques that enhance scaffold performance.

Recent developments in gradient scaffolds have focused on achieving highly controlled architectures, progressing from conventional squared and gyroid pore designs to more complex micro-truss structures, which better mimic the mechanical properties of OC tissue. Furthermore, the accuracy of SLA/DLP printing, reaching resolutions as fine as 10 μm, enables the fabrication of intricate structural gradients with unprecedented precision. Further advancements include multi-material printing systems, such as multi-material stereolithography (MMSL), which allow simultaneous deposition of different materials by adjusting light power densities. This approach enhances interface strength within scaffolds while preventing delamination. Moreover, combining VPP techniques with FDM or incorporating hydrogel infill has proven effective in decoupling mechanical and biochemical requirements, thereby improving scaffold-cell interactions.

Material selection plays a crucial role in scaffold performance, with blends of natural and synthetic polymers (*e.g.*, GelMA, PEGDA) and inorganic fillers (*e.g.*, HA, β-TCP) offering an optimal balance between resin viscosity, mechanical strength, degradation rate, and biocompatibility. Additionally, functionalizing synthetic polymers allows fine-tuning of scaffold properties by modifying their chemical structure and molecular weight. Recent studies have pushed the boundaries of biomimicry by integrating bioactive factors and extracellular matrix components, further enhancing cell adhesion, proliferation, and tissue regeneration.

6.2. Current challenges and future perspectives

Despite these advancements, several challenges remain, which limit the commercial and clinical adoption of OC gradient scaffolds.

Based on the reviewed literature, the authors believe that several aspects, particularly those related to *in vitro* and *in vivo* (in animal models) characterization, should be improved to enable a more accurate evaluation of newly developed products, which could, in turn, drive a reassessment of scaffold design for enhanced performance. For instance, little attention has been given so far to: 1) verifying scaffold stability to an adequate sterilization process, which is mandatory for clinical application; in this regard, the absence of cytotoxic leachables after sterilization should also be assessed; 2) evaluating the long-term stability (to chemical or, if the case, to enzymatically catalysed hydrolysis) of the device; and 3) assessing the scaffold's mechanical performance when equilibrated in physiological conditions, as hydration can significantly affect the material's mechanical behaviour. These evaluations should be standardized and, in addition to improving scaffold design and performance, would be valuable in developing a more comprehensive framework for subsequent device evaluation, particularly in preparation for commercial approval. Improved *in-vitro* characterization could help to reduce the high cost of *in vivo* experiments (on animal models) and an overall improved preclinical evaluation could help speed up the device optimization for the subsequent studies [156,157].

Secondly, achieving manufacturing scalability and reproducibility is a further problem, as batch-to-batch variability (*e.g.*, raw material purity and composition, processing conditions) can affect material properties and scaffold architecture, leading to inconsistent mechanical strength, porosity, biocompatibility, degradation kinetics, immune responses, and potential in supporting tissue regeneration.

Afterward, regulatory and approval barriers even more complicate the translation of these scaffolds into clinical settings. Like other Tissue Engineered Medical Products (TEMPs), OC scaffolds are classified as Class III (high-risk) medical devices by the EMA (European Medicines Agency) and the FDA (Food and Drug Administration) regulatory agencies, due to prolonged contact with biological tissues and potential biological effects. This classification requires a rigorous preclinical validation process, including predictive animal models, to ensure safety and efficacy prior to clinical testing. Generating robust preclinical data is key for securing funding to support applications for clinical trials. The latter, that typically consist of multiple phases, must demonstrate both the effectiveness and long-term safety of the device for final approval. Currently, medical devices manufactured using 3D printing technologies are subject to the same regulatory requirements as those produced through conventional manufacturing method. However, in case of 3D-printed medical devices, additional clinical information may be needed [156,158–160]. When considering application for OC regeneration, the overall process may be even more demanding than for other TEMPs due to the complexity of the device, which incorporate multiple materials and the cruciality of the biomechanical performance of the interface. Consequently, preclinical studies require more extensive testing of mechanical properties and biocompatibility, while clinical trials generally require extended follow-up [157,161,162].

A comprehensive understanding of the regulatory hurdles must also consider country variations in approval requirements and that the incorporation of biological components into the scaffold may change the classification into biologic/combined products further complicating regulatory approval [157,158]. It is therefore clear, based on the above, that the overall Premarket Approval process for 3D-printed OC scaffolds is highly costly and time-consuming, limiting investment potential and constraining innovation in this field [163].

After approval, the clinical adoption of 3D-printed OC devices faces additional challenges. The high costs associated with advanced technologies needed and the stringent regulatory testing obviously result in expensive products, with limited accessibility [159]. Moreover, persistent concerns regarding the long-term clinical efficacy of OC devices, along with limited familiarity of physicians with these emerging technologies and therapeutic approaches further contribute to slowing down the integration of the devices into clinical practice [157]. These are, therefore, additional challenges that must be addressed to ensure that these innovations can achieve their potential to improve patient health

outcomes.

Thus, future research should aim to address these limitations by optimizing scaffold designs for clinical applications, refining long-term functional assessments, standardizing fabrication and evaluation methodologies, and integrating quality control protocols, traceability of all process parameters and in-line or real-time analytics to monitor over production variability. These measures will be able support the development of reliable, high-quality products suitable for regulatory approval and widespread use. Moreover, combining DoE approaches and AI-driven computational methods with VPP techniques could significantly enhance the efficiency of scaffold development, reducing the number of required experiments while refining compositional, structural, and mechanical gradients, thus allowing to more closely mimic the architecture and functionality of OC tissues. Advancing these strategies will be essential for the widespread adoption of gradient OC scaffolds, ultimately bringing them closer to clinical translation in regenerative medicine.

CRediT authorship contribution statement

Federica Corrado: Writing – original draft, Investigation, Formal analysis, Data curation, Conceptualization. **Luciano Di Maio:** Supervision, Project administration, Formal analysis, Conceptualization. **Paola Palmero:** Validation, Funding acquisition. **Bartolomeo Coppola:** Validation, Methodology. **Zahid Abbas:** Investigation. **Annalisa La Gatta:** Visualization, Methodology. **Chiara Schiraldi:** Supervision. **Paola Scarfato:** Writing – review & editing, Visualization, Supervision, Resources, Project administration, Funding acquisition.

Declaration of competing interest

The authors declare that they have no known competing financial interests or personal relationships that could have appeared to influence the work reported in this paper.

Acknowledgements

We acknowledge financial support under the National Recovery and Resilience Plan (NRRP), Mission 4, Component 2, Investment 1.1, Call for tender No 104 published on 2.2.2022 by the Italian Ministry of University and Research (MUR), funded by the European Union – NextGenerationEU – Project 20228JPCTY - Title - DEsign and Stereolithography of cell-Instructive gradient scaffolds for osteochondral (DESIRE) – CUP D53D23005310006 - Grant Assignment Decree No 966 adopted on 30–06–2023 by the Italian Ministry of University and Research (MUR).

References

[1] J. Du, Z. Zhu, J. Liu, X. Bao, Q. Wang, C. Shi, C. Zhao, G. Xu, D. Li, 3D-printed gradient scaffolds for osteochondral defects: current status and perspectives, Int. J. Bioprinting 9 (2023) 724, https://doi.org/10.18063/ijb.724.

[2] N.A. Chartrain, C.B. Williams, A.R. Whittington, A review on fabricating tissue scaffolds using vat photopolymerization, Acta Biomater. 74 (2018) 90–111, https://doi.org/10.1016/j.actbio.2018.05.010.

[3] J.M. Oliveira, V.P. Ribeiro, R.L. Reis, Advances on gradient scaffolds for osteochondral tissue engineering, Prog. Biomed. Eng. 3 (2021) 033001, https://doi.org/10.1088/2516-1091/abfc2c.

[4] A. Pattnaik, A.S. Sanket, S. Pradhan, R. Sahoo, S. Das, S. Pany, T.E.L. Douglas, R. Dandela, Q. Liu, J. Rajadas, S. Pati, S.C. De Smedt, K. Braeckmans, S.K. Samal, Designing of gradient scaffolds and their applications in tissue regeneration, Biomaterials 296 (2023) 122078, https://doi.org/10.1016/j.biomaterials.2023.122078.

[5] X. Niu, N. Li, Z. Du, X. Li, Integrated gradient tissue-engineered osteochondral scaffolds: challenges, current efforts and future perspectives, Bioact. Mater. 20 (2023) 574–597, https://doi.org/10.1016/j.bioactmat.2022.06.011.

[6] S. Ansari, S. Khorshidi, A. Karkhaneh, Engineering of gradient osteochondral tissue: from nature to lab, Acta Biomater. 87 (2019) 41–54, https://doi.org/10.1016/j.actbio.2019.01.071.

[7] L. Chen, L. Wei, X. Su, L. Qin, Z. Xu, X. Huang, H. Chen, N. Hu, Preparation and characterization of biomimetic functional scaffold with gradient structure for osteochondral defect repair, Bioengineering 10 (2023) 213, https://doi.org/10.3390/bioengineering10020213.

[8] W. Xu, J. Zhu, J. Hu, L. Xiao, Engineering the biomechanical microenvironment of chondrocytes towards articular cartilage tissue engineering, Life Sci. 309 (2022) 121043, https://doi.org/10.1016/j.lfs.2022.121043.

[9] A. Di Luca, K. Szlazak, I. Lorenzo-Moldero, C.A. Ghebes, A. Lepedda, W. Swieszkowski, C. Van Blitterswijk, L. Moroni, Influencing chondrogenic differentiation of human mesenchymal stromal cells in scaffolds displaying a structural gradient in pore size, Acta Biomater. 36 (2016) 210–219, https://doi.org/10.1016/j.actbio.2016.03.014.

[10] T.E. Orr, P.A. Villars, S.L. Mitchell, H.-P. Hsu, M. Spector, Compressive properties of cancellous bone defects in a rabbit model treated with particles of natural bone mineral and synthetic hydroxyapatite, Biomaterials 22 (2001) 1953–1959, https://doi.org/10.1016/S0142-9612(00)00370-7.

[11] I. Martin, S. Miot, A. Barbero, M. Jakob, D. Wendt, Osteochondral tissue engineering, J. Biomech. 40 (2007) 750–765, https://doi.org/10.1016/j.jbiomech.2006.03.008.

[12] A.J. Krych, D.B.F. Saris, M.J. Stuart, B. Hacken, Cartilage injury in the knee: assessment and treatment options, JAAOS - J. Am. Acad. Orthop. Surg 28 (2020) 914, https://doi.org/10.5435/JAAOS-D-20-00266.

[13] C.-Y. Lin, Y.-L. Wang, Y.-J. Chen, C.-T. Ho, Y.-H. Chi, L.Y. Chan, G.-W. Chen, H.-C. Hsu, D.W. Hwang, H.-C. Wu, S.-C. Hung, Collagen-binding peptides for the enhanced imaging, lubrication and regeneration of osteoarthritic articular cartilage, Nat. Biomed. Eng. 6 (2022) 1105–1117, https://doi.org/10.1038/s41551-022-00948-5.

[14] N.K. Arden, T.A. Perry, R.R. Bannuru, O. Bruyère, C. Cooper, I.K. Haugen, M. C. Hochberg, T.E. McAlindon, A. Mobasheri, J.-Y. Reginster, Non-surgical management of knee osteoarthritis: comparison of ESCEO and OARSI 2019 guidelines, Nat. Rev. Rheumatol. 17 (2021) 59–66, https://doi.org/10.1038/s41584-020-00523-9.

[15] A. Bedi, B.T. Feeley, R.J.I. Williams, Management of articular cartilage defects of the knee, JBJS 92 (2010) 994, https://doi.org/10.2106/JBJS.I.00895.

[16] E.V. Medvedeva, E.A. Grebenik, S.N. Gornostaeva, V.I. Telpuhov, A.V. Lychagin, P.S. Timashev, A.S. Chagin, Repair of damaged articular cartilage: current approaches and future directions, Int. J. Mol. Sci. 19 (2018) 2366, https://doi.org/10.3390/ijms19082366.

[17] F. Zeifang, D. Oberle, C. Nierhoff, W. Richter, B. Moradi, H. Schmitt, Autologous chondrocyte implantation using the original periosteum-cover technique *versus* matrix-associated Autologous chondrocyte implantation: a randomized clinical trial, Am. J. Sports Med. 38 (2010) 924–933, https://doi.org/10.1177/0363546509351499.

[18] H. Madry, Surgical therapy in osteoarthritis, OsteoArthritis Cartilage 30 (2022) 1019–1034, https://doi.org/10.1016/j.joca.2022.01.012.

[19] E.A. Makris, A.H. Gomoll, K.N. Malizos, J.C. Hu, K.A. Athanasiou, Repair and tissue engineering techniques for articular cartilage, Nat. Rev. Rheumatol. 11 (2015) 21–34, https://doi.org/10.1038/nrrheum.2014.157.

[20] K. Rodríguez, S. Renneckar, P. Gatenholm, Biomimetic calcium phosphate crystal mineralization on electrospun cellulose-based scaffolds, ACS. Appl. Mater. Interfaces. 3 (2011) 681–689, https://doi.org/10.1021/am100972r.

[21] W. Lu, J. Sun, X. Jiang, Recent advances in electrospinning technology and biomedical applications of electrospun fibers, J. Mater. Chem. B 2 (2014) 2369–2380, https://doi.org/10.1039/C3TB21478H.

[22] B. Cong, H. Zhang, Innovative 3D printing technologies and advanced materials revolutionizing orthopedic surgery: current applications and future directions, Front. Bioeng. Biotechnol. 13 (2025), https://doi.org/10.3389/fbioe.2025.1542179.

[23] S.L. Sing, S. Wang, S. Agarwala, F.E. Wiria, T.M.H. Ha, W.Y. Yeong, Fabrication of titanium based biphasic scaffold using selective laser melting and collagen immersion, Int. J. Bioprinting 3 (2017) 007, https://doi.org/10.18063/IIB.2017.01.007.

[24] C.-C. Wong, C.-X. Lu, E.-C. Cho, P.-W. Lee, N.-W. Chi, P.-Y. Lin, P.-R. Jheng, H.-L. Chen, B.W. Mansel, Y.-M. Chen, C.-H. Chen, E.-Y. Chuang, Calcium peroxide aids tyramine-alginate gel to crosslink with tyrosinase for efficient cartilage repair, Int. J. Biol. Macromol. 208 (2022) 299–313, https://doi.org/10.1016/j.ijbiomac.2022.03.044.

[25] L. Yu, S. Cavelier, B. Hannon, M. Wei, Recent development in multizonal scaffolds for osteochondral regeneration, Bioact. Mater. 25 (2023) 122–159, https://doi.org/10.1016/j.bioactmat.2023.01.012.

[26] R. Lanza, R. Langer, J.P. Vacanti, A. Atala, Principles of Tissue Engineering, Academic Press, 2020.

[27] R. Pecci, S. Baiguera, P. Ioppolo, R. Bedini, C. Del Gaudio, 3D printed scaffolds with random microarchitecture for bone tissue engineering applications: manufacturing and characterization, J. Mech. Behav. Biomed. Mater. 103 (2020) 103583, https://doi.org/10.1016/j.jmbbm.2019.103583.

[28] D.Y. Park, S.-H. Kim, S.-H. Park, J.S. Jang, J.J. Yoo, S.J. Lee, 3D Bioprinting strategies for articular cartilage tissue engineering, Ann. Biomed. Eng. 52 (2024) 1883–1893, https://doi.org/10.1007/s10439-023-03236-8.

[29] Y. Du, H. Liu, Q. Yang, S. Wang, J. Wang, J. Ma, I. Noh, A.G. Mikos, S. Zhang, Selective laser sintering scaffold with hierarchical architecture and gradient composition for osteochondral repair in rabbits, Biomaterials 137 (2017) 37–48, https://doi.org/10.1016/j.biomaterials.2017.05.021.

[30] V. Zumstein, M. Kraljević, D. Wirz, R. Hügli, M. Müller-Gerbl, Correlation between mineralization and mechanical strength of the subchondral bone plate of the humeral head, J. Shoulder. Elbow. Surg. 21 (2012) 887–893, https://doi.org/10.1016/j.jse.2011.05.018.

[31] J. Xue, J. Xie, W. Liu, Y. Xia, Electrospun nanofibers: new concepts, materials, and applications, Acc. Chem. Res. 50 (2017) 1976–1987, https://doi.org/10.1021/acs.accounts.7b00218.
[32] J. Xue, T. Wu, Y. Dai, Y. Xia, Electrospinning and electrospun nanofibers: methods, materials, and applications, Chem. Rev. 119 (2019) 5298–5415, https://doi.org/10.1021/acs.chemrev.8b00593.
[33] A.R. do, V. Morais, É. do N. Alencar, F.H. Xavier Júnior, C.M. de Oliveira, H. R. Marcelino, G. Barratt, H. Fessi, E.S.T. do Egito, A. Elaissari, Freeze-drying of emulsified systems: a review, Int. J. Pharm. 503 (2016) 102–114, https://doi.org/10.1016/j.ijpharm.2016.02.047.
[34] Y. Zhu, H. Wu, S. Sun, T. Zhou, J. Wu, Y. Wan, Designed composites for mimicking compressive mechanical properties of articular cartilage matrix, J. Mech. Behav. Biomed. Mater. 36 (2014) 32–46, https://doi.org/10.1016/j.jmbbm.2014.04.003.
[35] S. Zhang, L. Chen, Y. Jiang, Y. Cai, G. Xu, T. Tong, W. Zhang, L. Wang, J. Ji, P. Shi, H.W. Ouyang, Bi-layer collagen/microporous electrospun nanofiber scaffold improves the osteochondral regeneration, Acta Biomater. 9 (2013) 7236–7247, https://doi.org/10.1016/j.actbio.2013.04.003.
[36] S. Reed, G. Lau, B. Delattre, D.D. Lopez, A.P. Tomsia, B.M. Wu, Macro- and micro-designed chitosan-alginate scaffold architecture by three-dimensional printing and directional freezing, Biofabrication. 8 (2016) 015003, https://doi.org/10.1088/1758-5090/8/1/015003.
[37] J. Idaszek, M. Costantini, T.A. Karlsen, J. Jaroszewicz, C. Colosi, S. Testa, E. Fornetti, S. Bernardini, M. Seta, K. Kasarełło, R. Wrzesień, S. Cannata, A. Barbetta, C. Gargioli, J.E. Brinchman, W. Święszkowski, 3D bioprinting of hydrogel constructs with cell and material gradients for the regeneration of full-thickness chondral defect using a microfluidic printing head, Biofabrication. 11 (2019) 044101, https://doi.org/10.1088/1758-5090/ab2622.
[38] M. Costantini, J. Jaroszewicz, Ł. Kozoń, K. Szlązak, W. Święszkowski, P. Garstecki, C. Stubenrauch, A. Barbetta, J. Guzowski, 3D-Printing of functionally graded porous materials using on-demand reconfigurable microfluidics, Angew. Chem. Int. Ed. 58 (2019) 7620–7625, https://doi.org/10.1002/anie.201900530.
[39] C. Li, L. Ouyang, I.J. Pence, A.C. Moore, Y. Lin, C.W. Winter, J.P.K. Armstrong, M. M. Stevens, Buoyancy-driven gradients for biomaterial fabrication and tissue engineering, Adv. Mater. 31 (2019) 1900291, https://doi.org/10.1002/adma.201900291.
[40] C. Li, J.P.K. Armstrong, I.J. Pence, W. Kit-Anan, J.L. Puetzer, S. Correia Carreira, A.C. Moore, M.M. Stevens, Glycosylated superparamagnetic nanoparticle gradients for osteochondral tissue engineering, Biomaterials 176 (2018) 24–33, https://doi.org/10.1016/j.biomaterials.2018.05.029.
[41] Z. Wu, H. Yao, H. Sun, Z. Gu, X. Hu, J. Yang, J. Shi, H. Yang, J. Dai, H. Chong, D.-A. Wang, L. Lin, W. Zhang, Enhanced hyaline cartilage formation and continuous osteochondral regeneration via 3D-printed heterogeneous hydrogel with multi-crosslinking inks, Mater. Today Bio 26 (2024) 101080, https://doi.org/10.1016/j.mtbio.2024.101080.
[42] A.M. Gonçalves, A. Moreira, A. Weber, G.R. Williams, P.F. Costa, Osteochondral tissue engineering: the potential of electrospinning and additive manufacturing, Pharmaceutics. 13 (2021) 983, https://doi.org/10.3390/pharmaceutics13070983.
[43] C. Maibohm, O.F. Silvestre, J. Borme, M. Sinou, K. Heggarty, J.B. Nieder, Multi-beam two-photon polymerization for fast large area 3D periodic structure fabrication for bioapplications, Sci. Rep. 10 (2020) 8740, https://doi.org/10.1038/s41598-020-64955-9.
[44] A. Zhakeyev, P. Wang, L. Zhang, W. Shu, H. Wang, J. Xuan, Additive manufacturing: unlocking the evolution of energy materials, Adv. Sci. 4 (2017) 1700187, https://doi.org/10.1002/advs.201700187.
[45] R. Winarso, P.W. Anggoro, R. Ismail, J. Jamari, A.P. Bayuseno, Application of fused deposition modeling (FDM) on bone scaffold manufacturing process: a review, Heliyon. 8 (2022), https://doi.org/10.1016/j.heliyon.2022.e11701.
[46] J.C. Najmon, S. Raeisi, A. Tovar, Review of additive manufacturing technologies and applications in the aerospace industry, in: F. Froes, R. Boyer (Eds.), Addit. Manuf. Aerosp. Ind, Elsevier, 2019, pp. 7–31, https://doi.org/10.1016/B978-0-12-814062-8.00002-9.
[47] D.-E. Radulescu, I.A. Neacsu, A.-M. Grumezescu, E. Andronescu, Novel trends into the development of natural hydroxyapatite-based polymeric composites for bone tissue engineering, Polymers. (Basel) 14 (2022) 899, https://doi.org/10.3390/polym14050899.
[48] H.S. Ghazali, E. Askari, Z.S. Ghazali, S.M. Naghib, T. Braschler, Lithography-based 3D printed hydrogels: from bioresin designing to biomedical application, Colloid. Interface Sci. Commun. 50 (2022) 100667, https://doi.org/10.1016/j.colcom.2022.100667.
[49] S.H. Moon, H.J. Hwang, H.R. Jeon, S.J. Park, I.S. Bae, Y.J. Yang, Photocrosslinkable natural polymers in tissue engineering, Front. Bioeng. Biotechnol. 11 (2023), https://doi.org/10.3389/fbioe.2023.1127757.
[50] J.-N. Fu, X. Wang, M. Yang, Y.-R. Chen, J.-Y. Zhang, R.-H. Deng, Z.-N. Zhang, J.-K. Yu, F.-Z. Yuan, Scaffold-based tissue engineering strategies for osteochondral repair, Front. Bioeng. Biotechnol. 9 (2022), https://doi.org/10.3389/fbioe.2021.812383.
[51] T.A.E. Ahmed, M.T. Hincke, Mesenchymal stem cell - based tissue engineering strategies for repair of articular cartilage, (2014). https://digitum.um.es/digitum/handle/10201/70698 (accessed July 24, 2024).
[52] T. Cao, K.-H. Ho, S.-H. Teoh, Scaffold design and *in vitro* study of osteochondral coculture in a three-dimensional porous polycaprolactone Scaffold fabricated by fused deposition modeling, Tissue Eng. 9 (2003) 103–112, https://doi.org/10.1089/10763270360697012.
[53] C.I. Codrea, D. Baykara, R.-A. Mitran, A.C.Ç. Koyuncu, O. Gunduz, A. Ficai, 3D-Bioprinted gelatin methacryloyl-strontium-doped hydroxyapatite composite hydrogels scaffolds for bone tissue regeneration, Polymers (Basel) 16 (2024) 1932, https://doi.org/10.3390/polym16131932.
[54] W. Guo, B. Li, P. Li, L. Zhao, H. You, Y. Long, Review on vat photopolymerization additive manufacturing of bioactive ceramic bone scaffolds, J. Mater. Chem. B 11 (2023) 9572–9596, https://doi.org/10.1039/D3TB01236K.
[55] W. Guo, L. Zhao, P. Li, E. Wang, Y. Pang, Y. Wei, B. Li, Y. Huang, B. Liu, S. Wang, H. You, Y. Long, All-natural ceramic composite bone scaffolds of whitlockite/wollastonite fibers: DLP additive manufacturing, microstructure, and performance, J. Mater. Res. Technol. 33 (2024) 7391–7405, https://doi.org/10.1016/j.jmrt.2024.11.077.
[56] W. Guo, P. Li, Y. Wei, L. Zhao, Y. Pang, Y. Huang, X. Ye, S. Wang, B. Liu, H. You, Y. Long, Ionic substitution through bredigite doping for microstructure and performance adjustment in DLP 3D-printed TPMS porous HA bone scaffolds, Virtual. Phys. Prototyp. 19 (2024) e2423840, https://doi.org/10.1080/17452759.2024.2423840.
[57] S.-J. Seo, C. Mahapatra, R.K. Singh, J.C. Knowles, H.-W. Kim, Strategies for osteochondral repair: focus on scaffolds, J. Tissue Eng. 5 (2014) 2041731414541850, https://doi.org/10.1177/2041731414541850.
[58] S. Hashemi, L.M. Amirabad, F.D. Nazhvani, P. Zarrintaj, H. Namazi, A. Saadatfar, A. Golchin, Bilayer scaffolds for Interface tissue engineering and Regenerative Medicine: a systematic reviews, in: K. Turksen (Ed.), Cell Biol. Transl. Med. Vol. 14 Stem Cells Lineage Specif. Differ. Dis., Springer International Publishing, Cham, 2021, pp. 83–113, https://doi.org/10.1007/5584_2021_637.
[59] C. Bertsch, H. Maréchal, V. Gribova, B. Lévy, C. Debry, P. Lavalle, L. Fath, Biomimetic bilayered scaffolds for tissue engineering: from current design strategies to medical applications, Adv. Healthc. Mater. 12 (2023) 2203115, https://doi.org/10.1002/adhm.202203115.
[60] T.M. O'Shea, X. Miao, Bilayered scaffolds for osteochondral tissue engineering, Tissue Eng. Part B Rev. 14 (2008) 447–464, https://doi.org/10.1089/ten.teb.2008.0327.
[61] C.-H. Chang, F.-H. Lin, C.-C. Lin, C.-H. Chou, H.-C. Liu, Cartilage tissue engineering on the surface of a novel gelatin–calcium-phosphate biphasic scaffold in a double-chamber bioreactor, J. Biomed. Mater. Res. B Appl. Biomater. 71B (2004) 313–321, https://doi.org/10.1002/jbm.b.30090.
[62] A. Bernhardt, B. Paul, M. Gelinsky, Biphasic scaffolds from marine collagens for regeneration of osteochondral defects, Mar. Drugs 16 (2018) 91, https://doi.org/10.3390/md16030091.
[63] J. Sun, J. Lyu, F. Xing, R. Chen, X. Duan, Z. Xiang, A biphasic, demineralized, and decellularized allograft bone-hydrogel scaffold with a cell-based BMP-7 delivery system for osteochondral defect regeneration, J. Biomed. Mater. Res. a 108 (2020) 1909–1921, https://doi.org/10.1002/jbm.a.36954.
[64] K. Klimek, A. Benko, M. Vandrovcova, M. Travnickova, T.E.L. Douglas, M. Tarczynska, A. Broz, K. Gaweda, G. Ginalska, L. Bacakova, Biomimetic biphasic curdlan-based scaffold for osteochondral tissue engineering applications – Characterization and preliminary evaluation of mesenchymal stem cell response *in vitro*, Biomater. Adv. 135 (2022) 212724, https://doi.org/10.1016/j.bioadv.2022.212724.
[65] W. Jiang, X. Xiang, M. Song, J. Shen, Z. Shi, W. Huang, H. Liu, An all-silk-derived bilayer hydrogel for osteochondral tissue engineering, Mater. Today Bio 17 (2022) 100485, https://doi.org/10.1016/j.mtbio.2022.100485.
[66] F. Donnaloja, E. Jacchetti, M. Soncini, M.T. Raimondi, Natural and synthetic polymers for bone scaffolds optimization, Polymers. (Basel) 12 (2020) 905. https://doi.org/10.3390/polym12040905.
[67] J. Reignier, M.A. Huneault, Preparation of interconnected poly(ε-caprolactone) porous scaffolds by a combination of polymer and salt particulate leaching, Polymer. (Guildf) 47 (2006) 4703–4717, https://doi.org/10.1016/j.polymer.2006.04.029.
[68] X. Guo, H. Park, G. Liu, W. Liu, Y. Cao, Y. Tabata, F.K. Kasper, A.G. Mikos, *In vitro* generation of an osteochondral construct using injectable hydrogel composites encapsulating rabbit marrow mesenchymal stem cells, Biomaterials 30 (2009) 2741–2752, https://doi.org/10.1016/j.biomaterials.2009.01.048.
[69] X. Zhao, X. Nie, X. Zhang, Y. Sun, R. Yang, X. Bian, Q. Zhang, H. Wang, Z. Xu, W. Liu, 3D printed β-sheet-reinforced natural polymer hydrogel bilayer tissue engineering scaffold, Sci. China Technol. Sci. 67 (2024) 1170–1184, https://doi.org/10.1007/s11431-023-2471-0.
[70] S.R. Goldring, M.B. Goldring, Changes in the osteochondral unit during osteoarthritis: structure, function and cartilage-bone crosstalk, Nat. Rev. Rheumatol. 12 (2016) 632–644, https://doi.org/10.1038/nrrheum.2016.148.
[71] A.-M. Yousefi, M.E. Hoque, R.G.S.V. Prasad, N. Uth, Current strategies in multiphasic scaffold design for osteochondral tissue engineering: a review, J. Biomed. Mater. Res. a 103 (2015) 2460–2481, https://doi.org/10.1002/jbm.a.35356.
[72] T.J. Levingstone, C. Moran, H.V. Almeida, D.J. Kelly, F.J. O'Brien, Layer-specific stem cell differentiation in tri-layered tissue engineering biomaterials: towards development of a single-stage cell-based approach for osteochondral defect repair, Mater. Today Bio 12 (2021) 100173, https://doi.org/10.1016/j.mtbio.2021.100173.
[73] H. Chen, J. Huang, X. Li, W. Zhao, Y. Hua, Z. Song, X. Wang, Z. Guo, G. Zhou, W. Ren, Y. Sun, Trilayered biomimetic hydrogel scaffolds with dual-differential microenvironment for articular osteochondral defect repair, Mater. Today Bio 26 (2024) 101051, https://doi.org/10.1016/j.mtbio.2024.101051.
[74] A. Tampieri, M. Sandri, E. Landi, D. Pressato, S. Francioli, R. Quarto, I. Martin, Design of graded biomimetic osteochondral composite scaffolds, Biomaterials 29 (2008) 3539–3546, https://doi.org/10.1016/j.biomaterials.2008.05.008.

[75] B. Zhang, J. Huang, R.J. Narayan, Gradient scaffolds for osteochondral tissue engineering and regeneration, J. Mater. Chem. B 8 (2020) 8149–8170, https://doi.org/10.1039/D0TB00688B.
[76] P. Nooeaid, V. Salih, J.P. Beier, A.R. Boccaccini, Osteochondral tissue engineering: scaffolds, stem cells and applications, J. Cell Mol. Med. 16 (2012) 2247–2270, https://doi.org/10.1111/j.1582-4934.2012.01571.x.
[77] P. Nooeaid, J.A. Roether, E. Weber, D.W. Schubert, A.R. Boccaccini, Technologies for multilayered scaffolds suitable for interface tissue engineering, Adv. Eng. Mater. 16 (2014) 319–327, https://doi.org/10.1002/adem.201300072.
[78] A. Di Luca, I. Lorenzo-Moldero, C. Mota, A. Lepedda, D. Auhl, C. Van Blitterswijk, L. Moroni, Tuning cell differentiation into a 3D scaffold presenting a pore shape gradient for osteochondral regeneration, Adv. Healthc. Mater. 5 (2016) 1753–1763, https://doi.org/10.1002/adhm.201600083.
[79] E. Amann, A. Amirall, A.R. Franco, P.S.P. Poh, F.J. Sola Dueñas, G. Fuentes Estévez, I.B. Leonor, R.L. Reis, M. van Griensven, E.R. Balmayor, A. Graded, Porous composite of natural biopolymers and octacalcium phosphate guides osteochondral differentiation of stem cells, Adv. Healthc. Mater. 10 (2021) 2001692, https://doi.org/10.1002/adhm.202001692.
[80] L.M. Cross, A. Thakur, N.A. Jalili, M. Detamore, A.K. Gaharwar, Nanoengineered biomaterials for repair and regeneration of orthopedic tissue interfaces, Acta Biomater. 42 (2016) 2–17, https://doi.org/10.1016/j.actbio.2016.06.023.
[81] J.M. Lowen, J.K. Leach, Functionally graded biomaterials for use as model systems and replacement tissues, Adv. Funct. Mater. 30 (2020) 1909089, https://doi.org/10.1002/adfm.201909089.
[82] C. Li, L. Ouyang, J.P.K. Armstrong, M.M. Stevens, Advances in the fabrication of biomaterials for gradient tissue engineering, Trends Biotechnol. 39 (2021) 150–164, https://doi.org/10.1016/j.tibtech.2020.06.005.
[83] J. Guo, C. Li, S. Ling, W. Huang, Y. Chen, D.L. Kaplan, Multiscale design and synthesis of biomimetic gradient protein/biosilica composites for interfacial tissue engineering, Biomaterials 145 (2017) 44–55, https://doi.org/10.1016/j.biomaterials.2017.08.025.
[84] M. Karimi, M. Asadi-Eydivand, N. Abolfathi, Y. Chehrehsaz, M. Solati-Hashjin, The effect of pore size and layout on mechanical and biological properties of 3D-printed bone scaffolds with gradient porosity, Polym. Compos. 44 (2023) 1343–1359. https://doi.org/10.1002/pc.27174.
[85] L. Guo, S. Ataollah Naghavi, Z. Wang, S. Nath Varma, Z. Han, Z. Yao, L. Wang, L. Wang, C. Liu, On the design evolution of hip implants: a review, Mater. Des. 216 (2022) 110552, https://doi.org/10.1016/j.matdes.2022.110552.
[86] K.C. Nune, R.D.K. Misra, S.M. Gaytan, L.E. Murr, Interplay between cellular activity and three-dimensional scaffold-cell constructs with different foam structure processed by electron beam melting, J. Biomed. Mater. Res. A 103 (2015) 1677–1692, https://doi.org/10.1002/jbm.a.35307.
[87] H. Shi, P. Zhou, J. Li, C. Liu, L. Wang, Functional gradient metallic biomaterials: techniques, current scenery, and future prospects in the biomedical field, Front. Bioeng. Biotechnol. 8 (2021), https://doi.org/10.3389/fbioe.2020.616845.
[88] Z. Zhao, J. Li, Y. Wei, T. Yu, Design and properties of graded polyamide12/hydroxyapatite scaffolds based on primitive lattices using selective laser sintering, J. Mech. Behav. Biomed. Mater. 126 (2022) 105052, https://doi.org/10.1016/j.jmbbm.2021.105052.
[89] X. Gu, Y. Zha, Y. Li, J. Chen, S. Liu, Y. Du, S. Zhang, J. Wang, Integrated polycaprolactone microsphere-based scaffolds with biomimetic hierarchy and tunable vascularization for osteochondral repair, Acta Biomater. 141 (2022) 190–197, https://doi.org/10.1016/j.actbio.2022.01.021.
[90] W. Lin, D. Chen, S.-C. Chen, Emerging micro-additive manufacturing technologies enabled by novel optical methods, Photonics. Res. 8 (2020) 1827–1842, https://doi.org/10.1364/PRJ.404334.
[91] Y.-W. Chen, M.-Y. Shie, W.-C. Chang, Y.-F. Shen, Approximate optimization study of light curing waterborne polyurethane materials for the construction of 3D printed cytocompatible cartilage scaffolds, Materials. (Basel) 14 (2021) 6804, https://doi.org/10.3390/ma14226804.
[92] A. Al Rashid, W. Ahmed, M.Y. Khalid, M. Koç, Vat photopolymerization of polymers and polymer composites: processes and applications, Addit. Manuf. 47 (2021) 102279, https://doi.org/10.1016/j.addma.2021.102279.
[93] L. Xiao, Y. Sun, L. Liao, X. Su, Response of mesenchymal stem cells to surface topography of scaffolds and the underlying mechanisms, J. Mater. Chem. B 11 (2023) 2550–2567, https://doi.org/10.1039/D2TB01875F.
[94] C.W. Hull, Apparatus for production of three-dimensional objects by stereolithography, US4575330A (1986). https://patents.google.com/patent/US4575330A/en (accessed July 24, 2024).
[95] F.P.W. Melchels, K. Bertoldi, R. Gabbrielli, A.H. Velders, J. Feijen, D.W. Grijpma, Mathematically defined tissue engineering scaffold architectures prepared by stereolithography, Biomaterials 31 (2010) 6909–6916, https://doi.org/10.1016/j.biomaterials.2010.05.068.
[96] F.P.W. Melchels, A.M.C. Barradas, C.A. van Blitterswijk, J. de Boer, J. Feijen, D. W. Grijpma, Effects of the architecture of tissue engineering scaffolds on cell seeding and culturing, Acta Biomater. 6 (2010) 4208–4217, https://doi.org/10.1016/j.actbio.2010.06.012.
[97] F.P.W. Melchels, B. Tonnarelli, A.L. Olivares, I. Martin, D. Lacroix, J. Feijen, D. J. Wendt, D.W. Grijpma, The influence of the scaffold design on the distribution of adhering cells after perfusion cell seeding, Biomaterials 32 (2011) 2878–2884, https://doi.org/10.1016/j.biomaterials.2011.01.023.
[98] W. Bian, D. Li, Q. Lian, X. Li, W. Zhang, K. Wang, Z. Jin, Fabrication of a bio-inspired beta-tricalcium phosphate/collagen scaffold based on ceramic stereolithography and gel casting for osteochondral tissue engineering, Rapid. Prototyp. J. 18 (2012) 68–80, https://doi.org/10.1108/13552541211193511.
[99] N.J. Castro, J. O'Brien, L.G. Zhang, Integrating biologically inspired nanomaterials and table-top stereolithography for 3D printed biomimetic osteochondral scaffolds, Nanoscale 7 (2015) 14010–14022, https://doi.org/10.1039/C5NR03425F.
[100] X. Wu, Q. Lian, D. Li, Z. Jin, Biphasic osteochondral scaffold fabrication using multi-material mask projection stereolithography, Rapid. Prototyp. J. 25 (2018) 277–288, https://doi.org/10.1108/RPJ-07-2017-0144.
[101] X. Zhou, T. Esworthy, S.-J. Lee, S. Miao, H. Cui, M. Plesiniak, H. Fenniri, T. Webster, R.D. Rao, L.G. Zhang, 3D Printed scaffolds with hierarchical biomimetic structure for osteochondral regeneration, Nanomed. Nanotechnol. Biol. Med. 19 (2019) 58–70, https://doi.org/10.1016/j.nano.2019.04.002.
[102] X. Zhou, S. Tenaglio, T. Esworthy, S.Y. Hann, H. Cui, T.J. Webster, H. Fenniri, L. G. Zhang, Three-dimensional printing biologically inspired DNA-based gradient scaffolds for cartilage tissue regeneration, ACS. Appl. Mater. Interfaces. 12 (2020) 33219–33228, https://doi.org/10.1021/acsami.0c07918.
[103] Z. Wang, C. Huang, J. Wang, B. Zou, C.A. Abbas, X. Wang, Design and characterization of hydroxyapatite scaffolds fabricated by stereolithography for bone tissue engineering application, Procedia CIRP. 89 (2020) 170–175, https://doi.org/10.1016/j.procir.2020.05.138.
[104] L.J. Hornbeck, Projection displays and MEMS: timely convergence for a bright future, Microelectron. Struct. Microelectromech.Dev. Opt. Process. Multimed. Appl. (1995), https://doi.org/10.1117/12.220929, 2–2.
[105] P. Chen, L. Zheng, Y. Wang, M. Tao, Z. Xie, C. Xia, C. Gu, J. Chen, P. Qiu, S. Mei, L. Ning, Y. Shi, C. Fang, S. Fan, X. Lin, Desktop-stereolithography 3D printing of a radially oriented extracellular matrix/mesenchymal stem cell exosome bioink for osteochondral defect regeneration, Theranostics. 9 (2019) 2439–2459, https://doi.org/10.7150/thno.31017.
[106] S. Jia, T. Zhang, Z. Xiong, W. Pan, J. Liu, W. Sun, *Vivo* evaluation of a novel oriented scaffold-BMSC construct for enhancing full-thickness articular cartilage repair in a rabbit model, PLoS. One 10 (2015) e0145667, https://doi.org/10.1371/journal.pone.0145667.
[107] Y. Zhang, F. Yang, K. Liu, H. Shen, Y. Zhu, W. Zhang, W. Liu, S. Wang, Y. Cao, G. Zhou, The impact of PLGA scaffold orientation on *in vitro* cartilage regeneration, Biomaterials 33 (2012) 2926–2935, https://doi.org/10.1016/j.biomaterials.2012.01.006.
[108] A. Arora, A. Kothari, D.S. Katti, Pore orientation mediated control of mechanical behavior of scaffolds and its application in cartilage-mimetic scaffold design, J. Mech. Behav. Biomed. Mater. 51 (2015) 169–183, https://doi.org/10.1016/j.jmbbm.2015.06.033.
[109] D. Xue, J. Zhang, Y. Wang, D. Mei, Digital light processing-based 3D printing of cell-seeding hydrogel scaffolds with regionally varied stiffness, ACS. Biomater. Sci. Eng. 5 (2019) 4825–4833, https://doi.org/10.1021/acsbiomaterials.9b00696.
[110] L. Gong, J. Li, J. Zhang, Z. Pan, Y. Liu, F. Zhou, Y. Hong, Y. Hu, Y. Gu, H. Ouyang, X. Zou, S. Zhang, An interleukin-4-loaded bi-layer 3D printed scaffold promotes osteochondral regeneration, Acta Biomater. 117 (2020) 246–260.
[111] S.A. Schoonraad, K.M. Fischenich, K.N. Eckstein, V. Crespo-Cuevas, L.M. Savard, A. Muralidharan, A.A. Tomaschke, A.C. Uzcategui, M.A. Randolph, R.R. McLeod, V.L. Ferguson, S.J. Bryant, Biomimetic and mechanically supportive 3D printed scaffolds for cartilage and osteochondral tissue engineering using photopolymers and digital light processing, Biofabrication. 13 (2021) 044106, https://doi.org/10.1088/1758-5090/ac23ab.
[112] K.N. Eckstein, J.E. Hergert, A.C. Uzcategui, S.A. Schoonraad, S.J. Bryant, R. R. McLeod, V.L. Ferguson, Controlled mechanical property gradients within a digital light processing printed hydrogel-composite osteochondral scaffold, Ann. Biomed. Eng. (2024), https://doi.org/10.1007/s10439-024-03516-x.
[113] M. Shirzad, A. Zolfagharian, A. Matbouei, M. Bodaghi, Design, evaluation, and optimization of 3D printed truss scaffolds for bone tissue engineering, J. Mech. Behav. Biomed. Mater. 120 (2021) 104594, https://doi.org/10.1016/j.jmbbm.2021.104594.
[114] D. Montgomery, C. St, Design and analysis of experiments, 9th Edition, 2022.
[115] G. Weisgrab, O. Guillaume, Z. Guo, P. Heimel, P. Slezak, A. Poot, D. Grijpma, A. Ovsianikov, 3D Printing of large-scale and highly porous biodegradable tissue engineering scaffolds from poly(trimethylene-carbonate) using two-photon-polymerization, Biofabrication. 12 (2020) 045036. https://doi.org/10.1088/1758-5090/abb539.
[116] N. Hauptmann, J. Ludolph, H. Rothe, J. Rost, A. Krupp, J. Lechner, S. Kohlhaas, M. Winkler, B. Stender, G. Hildebrand, K. Liefeith, Poly-alanine-ε-caprolacton-methacrylate as scaffold material with tuneable biomechanical properties for osteochondral implants, Int. J. Mol. Sci. 23 (2022) 3115, https://doi.org/10.3390/ijms23063115.
[117] A. Dobos, J. Van Hoorick, W. Steiger, P. Gruber, M. Markovic, O.G. Andriotis, A. Rohatschek, P. Dubruel, P.J. Thurner, S. Van Vlierberghe, S. Baudis, A. Ovsianikov, Thiol–Gelatin–Norbornene bioink for laser-based high-definition bioprinting, Adv. Healthc. Mater. 9 (2020) 1900752, https://doi.org/10.1002/adhm.201900752.
[118] T. Stichel, B. Hecht, R. Houbertz, G. Sextl, Two-photon polymerization as methode for the fabrication of large scale biomedical scaffold applications, J. Laser Micro Nanoeng. 5 (2010) 209–212, https://doi.org/10.2961/jlmn.2010.03.0005.
[119] X. Jing, H. Fu, B. Yu, M. Sun, L. Wang, Two-photon polymerization for 3D biomedical scaffolds: overview and updates, Front. Bioeng. Biotechnol. 10 (2022), https://doi.org/10.3389/fbioe.2022.994355.
[120] P. Timashev, Daria Kuznetsova, Anastasia Koroleva, Natalia Prodanets, Andrea Deiwick, Yuri Piskun, Ksenia Bardakova, Nina Dzhoyashvili, Sergei Kostjuk, Elena Zagaynova, Yuri Rochev, Chichkov, V. Boris, Bagratashvili,

Novel biodegradable star-shaped polylactide scaffolds for bone regeneration fabricated by two-photon polymerization, Nanomed 11 (2016) 1041–1053, https://doi.org/10.2217/nnm-2015-0022.
[121] R. Schade, T. Weiß, A. Berg, M. Schnabelrauch, K. Liefeith, Two-photon techniques in tissue engineering, Int. J. Artif. Organs 33 (2010) 219–227, https://doi.org/10.1177/039139881003300406.
[122] J. Gao, M. Li, J. Cheng, X. Liu, Z. Liu, J. Liu, P. Tang, 3D-Printed GelMA/PEGDA/F127DA scaffolds for bone regeneration, J. Funct. Biomater. 14 (2023) 96, https://doi.org/10.3390/jfb14020096.
[123] X. Zhang, Z. Yan, G. Guan, Z. Lu, S. Yan, A. Du, L. Wang, Q. Li, Polyethylene glycol diacrylate scaffold filled with cell-laden methacrylamide gelatin/alginate hydrogels used for cartilage repair, J. Biomater. Appl. 36 (2022) 1019–1032, https://doi.org/10.1177/08853282211044853.
[124] K. Yue, G. Trujillo-de Santiago, M.M. Alvarez, A. Tamayol, N. Annabi, A. Khademhosseini, Synthesis, properties, and biomedical applications of gelatin methacryloyl (GelMA) hydrogels, Biomaterials 73 (2015) 254–271, https://doi.org/10.1016/j.biomaterials.2015.08.045.
[125] B. Zhou, X. Jiang, X. Zhou, W. Tan, H. Luo, S. Lei, Y. Yang, GelMA-based bioactive hydrogel scaffolds with multiple bone defect repair functions: therapeutic strategies and recent advances, Biomater. Res. 27 (2023) 86, https://doi.org/10.1186/s40824-023-00422-6.
[126] Y. Wang, M. Ma, J. Wang, W. Zhang, W. Lu, Y. Gao, B. Zhang, Y. Guo, Development of a photo-crosslinking, biodegradable GelMA/PEGDA hydrogel for guided bone regeneration materials, Mater. Basel Switz. 11 (2018) 1345, https://doi.org/10.3390/ma11081345.
[127] M. Lee, R. Rizzo, F. Surman, M. Zenobi-Wong, Guiding lights: tissue bioprinting using photoactivated materials, Chem. Rev. 120 (2020) 10950–11027, https://doi.org/10.1021/acs.chemrev.0c00077.
[128] T.-U. Nguyen, K.E. Watkins, V. Kishore, Photochemically crosslinked cell-laden methacrylated collagen hydrogels with high cell viability and functionality, J. Biomed. Mater. Res. a 107 (2019) 1541–1550, https://doi.org/10.1002/jbm.a.36668.
[129] S. Benedikt, J. Wang, M. Markovic, N. Moszner, K. Dietliker, A. Ovsianikov, H. Grützmacher, R. Liska, Highly efficient water-soluble visible light photoinitiators, J. Polym. Sci. Part Polym. Chem. 54 (2016) 473–479, https://doi.org/10.1002/pola.27903.
[130] S. Wang, Y. Xiong, J. Lalevée, P. Xiao, J. Liu, F. Xing, Biocompatibility and cytotoxicity of novel photoinitiator π-conjugated dithienophosphole derivatives and their triggered polymers, Toxicol. In. Vitro 63 (2020) 104720, https://doi.org/10.1016/j.tiv.2019.104720.
[131] W. Tomal, J. Ortyl, Water-soluble photoinitiators in biomedical applications, Polymers (Basel) 12 (2020) 1073, https://doi.org/10.3390/polym12051073.
[132] F. Dumur, Recent advances on water-soluble photoinitiators of polymerization, Eur. Polym. J. 189 (2023) 111942, https://doi.org/10.1016/j.eurpolymj.2023.111942.
[133] F.P.W. Melchels, J. Feijen, D.W. Grijpma, A poly(d,l-lactide) resin for the preparation of tissue engineering scaffolds by stereolithography, Biomaterials 30 (2009) 3801–3809, https://doi.org/10.1016/j.biomaterials.2009.03.055.
[134] N. Barouh, C. Bourlieu-Lacanal, M.C. Figueroa-Espinoza, E. Durand, P. Villeneuve, Tocopherols as antioxidants in lipid-based systems: the combination of chemical and physicochemical interactions determines their efficiency, Compr. Rev. Food Sci. Food Saf. 21 (2022) 642–688, https://doi.org/10.1111/1541-4337.12867.
[135] Final report on the safety assessment of tocopherol, tocopheryl acetate, tocopheryl linoleate, tocopheryl linoleate/oleate, tocopheryl nicotinate, tocopheryl succinate, dioleyl tocopheryl methylsilanol, Potassium Ascorbyl Tocopheryl Phosphate Tocophersolan (2002) (n.d.), https://journals.sagepub.com/doi/abs/10.1080/10915810290169819 (accessed April 14, 2025).
[136] C.A. Murphy, K.S. Lim, T.B.F. Woodfield, Next evolution in organ-scale biofabrication: bioresin design for rapid high-resolution vat polymerization, Adv. Mater. 34 (2022) 2107759, https://doi.org/10.1002/adma.202107759.
[137] R.J. Mondschein, A. Kanitkar, C.B. Williams, S.S. Verbridge, T.E. Long, Polymer structure-property requirements for stereolithographic 3D printing of soft tissue engineering scaffolds, Biomaterials 140 (2017) 170–188, https://doi.org/10.1016/j.biomaterials.2017.06.005.
[138] A. Salas, M. Zanatta, V. Sans, I. Roppolo, Chemistry in light-induced 3D printing, ChemTexts. 9 (2023) 4, https://doi.org/10.1007/s40828-022-00176-z.
[139] T. Ishaq, R. Tehseen, U. Omer, A. Mustaqeem, R. Javaid, M. Mehr, M. Yousaf, Incremental learning with self-organizing Bayesian adaptive Incremental network (SOBAIN), J. Comput. Biomed. Inform. (2025). https://jcbi.org/index.php/Main/article/view/857 (accessed April 2, 2025).
[140] S. Abedin Dargoush, H. Hanaee-Ahvaz, S. Irani, M. Soleimani, S.M. Khatami, A. N. Sohi, A composite bilayer scaffold functionalized for osteochondral tissue regeneration in rat animal model, J. Tissue Eng. Regen. Med. 16 (2022) 559–574, https://doi.org/10.1002/term.3297.
[141] M. Krok-Borkowicz, K. Reczyńska, Ł. Rumian, E. Menaszek, M. Orzelski, P. Malisz, P. Silmanowicz, P. Dobrzyński, E. Pamuła, Surface-modified poly(l-lactide-co-glycolide) scaffolds for the treatment of osteochondral critical size defects—in vivo studies on rabbits, Int. J. Mol. Sci. 21 (2020) 7541, https://doi.org/10.3390/ijms21207541.
[142] S. Khod, M. Goswami, A. Dvivedi, Additive manufacturing processes protocol prediction by Artificial intelligence using X-ray computed tomography data, Prog. Addit. Manuf. (2025), https://doi.org/10.1007/s40964-025-01000-z.
[143] M. Bhattacharya, M. Penica, E. O'Connell, M. Hayes, AI-driven real-time failure detection in additive manufacturing, Procedia Comput. Sci. 232 (2024) 3229–3238, https://doi.org/10.1016/j.procs.2024.02.138.
[144] M. Gharibshahian, M. Torkashvand, M. Bavisi, N. Aldaghi, A. Alizadeh, Recent advances in artificial intelligent strategies for tissue engineering and regenerative medicine, Skin. Res. Technol. 30 (2024) e70016, https://doi.org/10.1111/srt.70016.
[145] E. Kolomenskaya, V. Butova, A. Poltavskiy, A. Soldatov, M. Butakova, Application of artificial intelligence at all stages of bone tissue engineering, Biomedicines. 12 (2024) 76, https://doi.org/10.3390/biomedicines12010076.
[146] S. Ibrahimi, L. D'Andrea, D. Gastaldi, M.W. Rivolta, P. Vena, Machine learning approaches for the design of biomechanically compatible bone tissue engineering scaffolds, Comput. Methods Appl. Mech. Eng. 423 (2024) 116842, https://doi.org/10.1016/j.cma.2024.116842.
[147] O. Jeznach, S. Tabakoglu, A. Zaszczyńska, P. Sajkiewicz, Review on machine learning application in tissue engineering: what has been done so far? Application areas, challenges, and perspectives, J. Mater. Sci. 59 (2024) 21222–21250, https://doi.org/10.1007/s10853-024-10449-2.
[148] S. Rafieyan, E. Ansari, E. Vasheghani-Farahani, A practical machine learning approach for predicting the quality of 3D (bio)printed scaffolds, Biofabrication. 16 (2024) 045014, https://doi.org/10.1088/1758-5090/ad6374.
[149] D. Ege, S. Sertturk, B. Acarkan, A. Ademoglu, Machine learning models to predict the relationship between printing parameters and tensile strength of 3D Poly (lactic acid) scaffolds for tissue engineering applications, Biomed. Phys. Eng. Express. 9 (2023) 065014, https://doi.org/10.1088/2057-1976/acf581.
[150] L.Y. Sujeeun, I.C. Phul, N. Goonoo, N.A. Kotov, A. Bhaw-Luximon, Predicting inflammatory response of biomimetic nanofibre scaffolds for tissue regeneration using machine learning and graph theory, J. Mater. Chem. B 13 (2025) 3304–3318, https://doi.org/10.1039/D4TB02494J.
[151] I.A.O. Beeren, P.J. Dijkstra, C. Mota, S. Camarero-Espinosa, M.B. Baker, L. Moroni, Advances in additive manufactured scaffolds mimicking the osteochondral interface, Adv. Nanobiomed. Res. 4 (2024) 2400059, https://doi.org/10.1002/anbr.202400059.
[152] J. Wu, Y. Zhang, Y. Lyu, L. Cheng, On the various numerical techniques for the optimization of bone scaffold, Materials (Basel) 16 (2023) 974, https://doi.org/10.3390/ma16030974.
[153] J. Kim, J.A. McKee, J.J. Fontenot, J.P. Jung, Engineering tissue fabrication with machine intelligence: generating a blueprint for regeneration, Front. Bioeng. Biotechnol. 7 (2020), https://doi.org/10.3389/fbioe.2019.00443.
[154] I. Sachdeva, S. Ramesh, U. Chadha, H. Punugoti, S.K. Selvaraj, Computational AI models in VAT photopolymerization: a review, current trends, open issues, and future opportunities, Neural Comput. Appl. 34 (2022) 17207–17229, https://doi.org/10.1007/s00521-022-07694-4.
[155] H. Xu, Q. Liu, J. Casillas, M. Mcanally, N. Mubtasim, L.S. Gollahon, D. Wu, C. Xu, Prediction of cell viability in dynamic optical projection stereolithography-based bioprinting using machine learning, J. Intell. Manuf. 33 (2022) 995–1005, https://doi.org/10.1007/s10845-020-01708-5.
[156] P. Karami, T. Stampoultzis, Y. Guo, D.P. Pioletti, A guide to preclinical evaluation of hydrogel-based devices for treatment of cartilage lesions, Acta Biomater. 158 (2023) 12–31, https://doi.org/10.1016/j.actbio.2023.01.015.
[157] C. Ai, Y.H.D. Lee, X.H. Tan, S.H.S. Tan, J.H.P. Hui, J.C.-H. Goh, Osteochondral tissue engineering: perspectives for clinical application and preclinical development, J. Orthop. Transl. 30 (2021) 93–102, https://doi.org/10.1016/j.jot.2021.07.008.
[158] M.P. Sekar, H. Budharaju, A. Zennifer, S. Sethuraman, N. Vermeulen, D. Sundaramurthi, D.M. Kalaskar, Current standards and ethical landscape of engineered tissues-3D bioprinting perspective, J. Tissue Eng. 12 (2021) 20417314211027677, https://doi.org/10.1177/20417314211027677.
[159] M.G. Bhise, L. Patel, K. Patel, 3D Printed medical devices: regulatory standards and technological advancements in the USA, Canada and Singapore-A cross-national study, Int. J. Pharm. Investig. 14 (2025) 888–902, https://doi.org/10.5530/ijpi.14.3.99.
[160] D1.1. Report on State of the art of osteochondral scaffolds and patent., n.d.
[161] D.S. Nedrelow, J.M. Townsend, M.S. Detamore, Osteochondral regeneration with anatomical scaffold 3D-printing—Design considerations for interface integration, J. Biomed. Mater. Res. a 113 (2025) e37804, https://doi.org/10.1002/jbm.a.37804.
[162] D. Bicho, S. Pina, R.L. Reis, J.M. Oliveira, Commercial products for osteochondral tissue repair and regeneration, in: J.M. Oliveira, S. Pina, R.L. Reis, J.San Roman (Eds.), Osteochondral Tissue Eng. Nanotechnol. Scaffolding-Relat. Dev. Transl, Springer International Publishing, Cham, 2018, pp. 415–428, https://doi.org/10.1007/978-3-319-76711-6_19.
[163] B.W. Yang, M.L. Iorio, C.S. Day, Orthopaedic device approval through the premarket approval process: a financial feasibility analysis for a single center, JBJS 99 (2017) e26, https://doi.org/10.2106/JBJS.16.00050.